TITLE: Host lipids regulate multicellular behavior of a predator of a human pathogen

Ria Q. Kidner[1], Eleanor B. Goldstone[1], Martina R. Laidemitt[2], Melissa C. Sanchez[2], Catherine Gerdt[1], Lorin P. Brokaw[1], Núria Ros-Rocher[3,4], Jamie Morris[5], W. Sean Davidson[5], & Joseph P. Gerdt[1]

[1]Department of Chemistry, Indiana University, Bloomington, IN 47405, USA.

[2]Department of Biology, Center for Evolutionary and Theoretical Immunology, Parasite Division, Museum of Southwestern Biology, University of New Mexico, Albuquerque, New Mexico 87131, USA.

[3]Department of Functional Genomics and Evolution, Institut de Biologia Evolutiva (Consejo Superior de Investigaciones Científicas-Universitat Pompeu Fabra), Passeig Marítim de la Barceloneta 37-49, 08003 Barcelona, Spain.

[4]Department of Cell Biology and Infection and Department of Developmental and Stem Cell Biology, Institut Pasteur, Université Paris-Cité, CNRS UMR3691, 25-28 Rue du Docteur Roux, 75015, Paris, France

[5] Department of Pathology and Laboratory Medicine, University of Cincinnati, Cincinnati OH 45237, USA.

ABSTRACT

As symbionts of animals, microbial eukaryotes benefit and harm their hosts in myriad ways. A model microeukaryote (*Capsaspora owczarzaki*) is a symbiont of *Biomphalaria glabrata* snails and may prevent transmission of parasitic schistosomes from snails to humans. However, it is unclear which host factors determine *Capsaspora*'s ability to colonize snails. Here, we discovered that *Capsaspora* forms multicellular aggregates when exposed to snail hemolymph. We identified a molecular cue for aggregation: a hemolymph-derived phosphatidylcholine, which becomes elevated in schistosome-infected snails. Therefore, *Capsaspora* aggregation may be a response to the physiological state of its host, and it may determine its ability to colonize snails and exclude parasitic schistosomes. Furthermore, *Capsaspora* is an evolutionary model organism whose aggregation may be ancestral to animals. This discovery, that a prevalent lipid induces *Capsaspora* multicellularity, suggests that this aggregation phenotype may be ancient. Additionally, the specific lipid will be a useful tool for further aggregation studies.

INTRODUCTION

32

33   Microbial symbionts frequently impact the fitness of their animal hosts—both for the better and

34   the worse.[1,2] Due to their abundance and ease of study, bacterial symbionts have garnered the

35   most research. However, microbial *eukaryotes* (*i.e.,* protists) also frequently influence their hosts.[3]

36   Although pathogens are the best studied eukaryotic symbionts (*e.g., Plasmodium, Leishmania,*

37   *Candida*, and chytrids),[4-7] mutualist and commensal microeukaryotes also populate the

38   literature.[8-10] The protist *Capsaspora owczarzaki* (hereafter "*Capsaspora*") is an intriguing

39   symbiont of snails that may *both* reveal insight into protist-animal symbioses *and* curtail the

40   spread of neglected tropical diseases.[11,12]

41   *Capsaspora* was initially isolated as unicellular filopodiated amoebae from the pericardia and

42   mantles of *Biomphalaria glabrata*. This snail is also the intermediate host that transmits

43   *Schistosoma mansoni,* the causative agent of intestinal human schistosomiasis in Africa and the

44   Neotropics (**Fig. 1A**).[11,12] Due to its disease relevance, *Biomphalaria* snails have been well studied

45   in the laboratory for decades.[13-17] More recently, *Capsaspora* has also become an emerging

46   experimental model with substantial "omic" resources[18-23] and molecular tools available,[24-27]

47   making this snail-amoeba symbiosis ideally suited for deeper analysis as a model system. More

48   significantly, *Capsaspora* can readily adhere to and kill schistosomes while they are sporocysts

49   (the intramolluscan growth stage) *in vitro*.[12,28] Therefore, *Capsaspora* may be able to halt the

50   spread of schistosomiasis by outcompeting schistosomes within their intermediate host snails—

51   similar to how *Wolbachia* bacteria halt the spread of mosquito-transmitted diseases.[29-31] Since the

52   ~300 million people who suffer snail-transmitted diseases can be difficult to treat, such an

53   ecological intervention to deplete parasites in endemic areas is an attractive approach.[32-34]

54   However, the interactions between *Capsaspora*, *Biomphalaria* snails, and schistosome parasites

55   are still poorly understood.[11,12,28,35]

56   Although *Capsaspora* has been isolated from multiple inbred lines of *B. glabrata*[11] and

57   molecularly detected by sequencing from wild snails,[36] it remains absent from many *B. glabrata*

58   snails in the laboratory and the wild. Moreover, it is unknown which host factors determine

59   *Capsaspora*'s ability to colonize the snail, and it is also unclear what fitness impact *Capsaspora*

60   has on its host snail and co-resident parasites. Additionally, multiple life stages of *Capsaspora*

61   have been described in the laboratory,[23] but it is unclear which life stages are relevant to its

62   behavior inside the host snail (**Fig. 1B**). In this study, we aimed to determine if *Capsaspora* could

63   respond to chemical or cellular factors in its host snail environment.

64   We found that within snail host tissue, *Capsaspora* formed multicellular aggregates. These

65   aggregates appeared similar to those formed by *Capsaspora* upon *in vitro* exposure to fetal

66   bovine serum.[27] Furthermore, we discovered that the aggregation inducer in the snail serum is a

67   specific phosphatidylcholine lipid (or possibly a suite of phosphatidylcholine lipids). Remarkably,

68   the concentration of this lipid in the snail hemolymph increased when the snail was infected with

69   schistosomes, which led to significantly greater *Capsaspora* aggregation. *Capsaspora* also

70   aggregated differently in hemolymph from different inbred snail lines. Therefore, *Capsaspora* can

71   sense and respond to the physiological state and identity of its host snail. This work raises the

72   hypothesis that a chemical mechanism of host discrimination may explain the presence of

73   *Capsaspora* in some snails but not others. Further dissection of its *in vivo* aggregation and

74   persistence may reveal the molecular requirements for *Capsaspora* to colonize its host and

75   possibly exclude pathogenic schistosomes.

76

RESULTS

Capsaspora forms multicellular aggregates in snail tissue

79   To obtain an initial glimpse into the interaction of *Capsaspora* with its host snail, we introduced

80   fluorescently labeled *Capsaspora* cells in the filopodial stage into naïve *Biomphalaria glabrata*

81   (NMRI) snails. The snails had no prior schistosome infection or colonization with *Capsaspora* (as

82   evidenced by PCR, see *Supporting Information* **Fig. S1A–B**). Since *Capsaspora* has been

83   isolated from snail pericardial explants and mantle explants and swabs,[12] we injected *Capsaspora*

84   cells into the pericardia and mantles. We discovered that *Capsaspora* formed multicellular

85   aggregates within 5 minutes of injection into the tissue (**Fig. 1C**, left and center images, **Fig. S1C–**

86   **D**). In contrast, *Capsaspora* imaged in the absence of snail tissue (in the injection buffer control)

87   failed to aggregate (**Fig. 1C**, right image), verifying that components of the snail triggered

88   *Capsaspora* aggregation. Notably, these aggregates were reminiscent of the aggregates

89   observed upon addition of fetal bovine serum (FBS) to *Capsaspora* cells *in vitro*.[27] Like FBS-

90   induced aggregation, this aggregation phenotype was calcium dependent: co-injection of excess

91   EGTA (a calcium-specific chelator) with *Capsaspora* into the snail pericardia and mantles

92   suppressed the aggregation phenotype (**Fig. 1D**). The observation of *Capsaspora* aggregation

93   inside its natural snail host suggests that *Capsaspora*'s previously-observed aggregation

94   phenotype may be ecologically relevant within the natural snail environment (not an artefact of

95   artificial *in vitro* growth media).
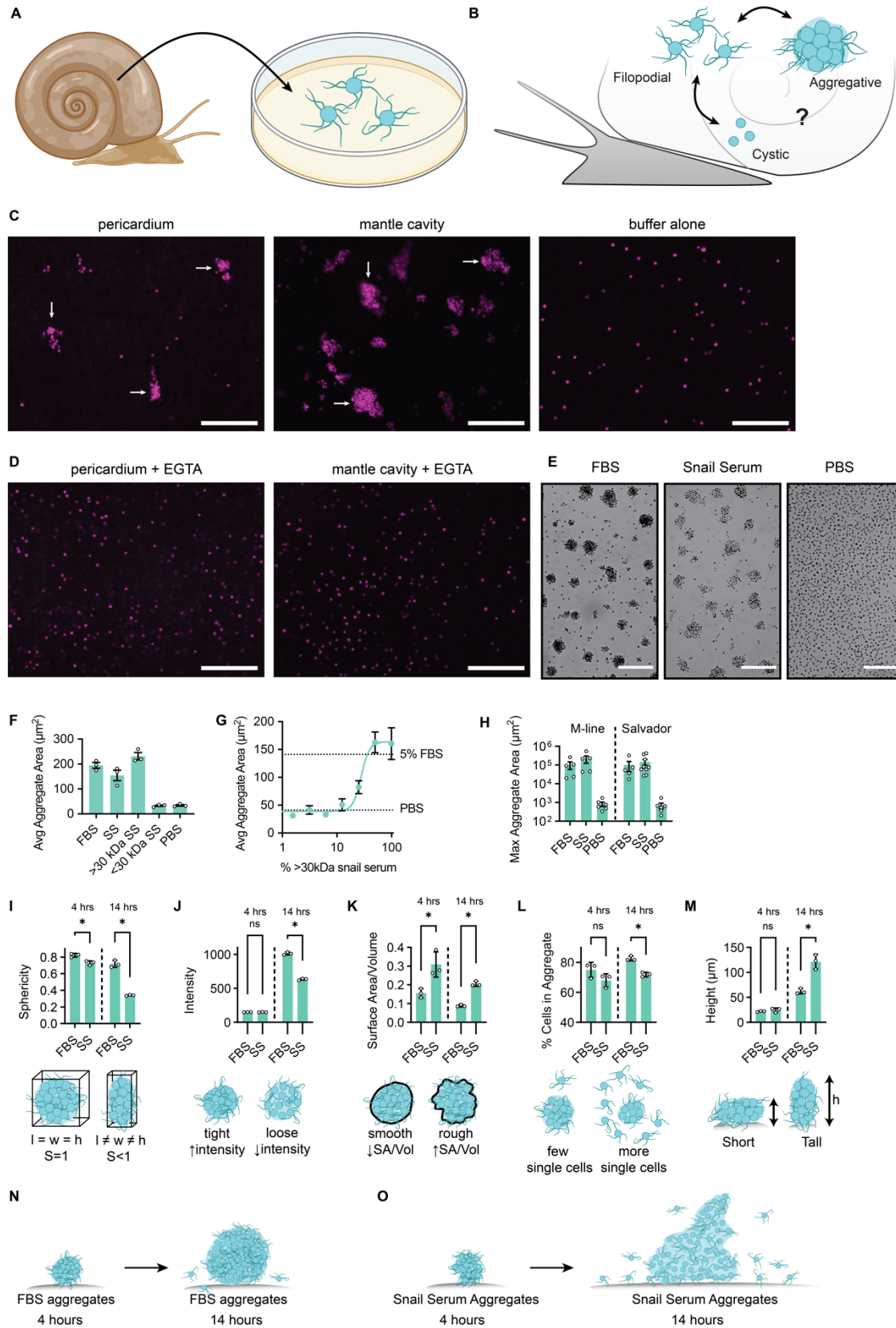
Figure 1. *Capsaspora* aggregates in response to snail tissue and serum. (A) *Capsaspora* was originally isolated from the pericardium and mantle of *B. glabrata*. Cells that grew out from snail samples were filopodiated. (B) Known *Capsaspora* life stages: filopodiated amoebae, cysts, and multicellular aggregates. It was previously unclear which life stages of *Capsaspora* are present inside snails. (C) Representative images of tdTomato-expressing *Capsaspora* (ATCC®30864) aggregates observed after injection into *B. glabrata* (NMRI) snail tissues (left and center images) compared to a negative control where *Capsaspora* was injected directly onto a microscope slide with no snail (right image). White arrows indicate example aggregates. (D) Representative images of *Capsaspora* co-injected with a calcium chelator (EGTA, 250 mM) into snail tissues—aggregation was prevented. (E) Representative images of *Capsaspora* aggregates induced by either 5% (v/v) FBS or 50% (v/v) snail serum compared to cells treated with 5% (v/v) 1X PBS buffer negative control. (F) Average area of cell aggregates induced by FBS, snail serum (SS), and small molecules (<30 kDa) and macromolecules (>30 kDa) from snail serum. (G) Dilution series of >30 kDa snail serum shows a dose-dependent induction of aggregation with an EC50 ~30% (v/v). (H) Area of aggregates induced by either 10% (v/v) FBS or 50% (v/v) >30 kDa snail serum in multiple isolated strains of *Capsaspora*. All strains tested showed aggregation in response to snail serum. (I–M) Analysis of 3D confocal microscopy images of *Capsaspora* cells after 4 hours and 14 hours of induction with either 5% (v/v) FBS or 50% (v/v) snail serum. Cells at 4 hours were tdTomato-expressing *Capsaspora*, and cells at 14 hours were stained with 0.02 mg/mL propidium iodide. (I) Sphericity of aggregates, determined by the ratio of aggregate bounding box dimensions. The average snail serum-induced aggregate was less spherical than FBS-induced aggregates. (J) The density of snail serum aggregates, calculated by the average intensity of stained-cell fluorescence, was similar to the density of FBS aggregates at 4 hours and lower than FBS aggregates at 14 hours. (K) The roughness of the aggregate surface, calculated by the surface area to volume ratio, was higher in snail serum aggregates at both time points. (L) The percentage of cells included within an aggregate, relative to the total number of cells in an image, showed there were slightly more non-aggregated cells present in snail serum-induced samples compared to those with FBS induction. This effect was more significant at 14 hours than 4 hours. (M) The average heights of the snail serum-induced aggregates were similar to the average FBS-induced aggregates at 4 hours but reached substantially taller by 14 hours. (N) Cartoons representing side views of typical aggregates induced by 5% (v/v) FBS at 4 hours and at 14 hours. (O) Cartoons representing side views of typical aggregates induced by 50% (v/v) snail serum at 4 hours and at 14 hours. Representative images of FBS-induced aggregates and snail serum-induced aggregates from a top-view and a side-view at 4 hours and 14 hours are

131   shown in **Fig. S2A–D**. For microscopy images, scale bars are 100 μm. For plots, mean ± sem

132   (n=3) are shown, and values from individual replicates are displayed with small circles.

133

Capsaspora forms multicellular aggregates in response to macromolecules in host snail serum

136   *Capsaspora* was also previously isolated from snail hemolymph.[11] Therefore, we asked

137   whether hemolymph alone could induce *Capsaspora* aggregation *in vitro*. Indeed, sterile-filtered

138   (0.22 μm) hemolymph from NMRI snails (hereafter "snail serum" or "SS") induced cellular

139   aggregation (**Fig. 1E–F**). Because the aggregate inducer previously found in FBS was a large

140   lipoprotein complex,[27] we hypothesized that the inducer in snail serum was a macromolecule. To

141   test this hypothesis, we fractionated snail serum using a 30 kDa MW cutoff filter, and the large

142   and small fractions were tested separately. As hypothesized, we found that >30 kDa snail serum

143   induced robust aggregation, and the <30 kDa fraction did not (**Fig. 1F**). Aggregation induced by

144   >30 kDa snail serum was dose-dependent with an EC50 ~30% (v/v) (**Fig. 1G**).

145   We also asked if the behavior was conserved across multiple isolates of *Capsaspora* (or if it

146   was possibly a phenotype unique to a single *Capsaspora* strain). In addition to the well-studied

147   ATCC 30864 *Capsaspora* strain, we tested the ability of snail serum to induce aggregation of two

148   other *Capsaspora* strains isolated separately from M-line and Salvador *B. glabrata* snails (ATCC

149   50973 and 50974, respectively).[11] Both of the alternative *Capsaspora* strains aggregated in

150   response to snail serum, as well as FBS (**Fig. 1H**). Notably, the other two cultures are less studied

151   and grow slower *in vitro*, possibly indicating less adaptation to laboratory culture conditions.

152   Therefore, we believe that the aggregative response of *Capsaspora* to *Biomphalaria* serum

153   components is likely a widespread and natural *Capsaspora* phenotype. The original ATCC 30864

154   strain was used for further studies in this manuscript.

155   Compared to previous reports of *Capsaspora* aggregation, we noticed that the snail serum-

156   induced aggregates appeared less circular and less dense than those induced by FBS. This

157   observation motivated us to characterize the aggregation morphology of *Capsaspora* cells

158   induced by snail serum compared to FBS-induced aggregates via confocal microscopy. We

159   assessed both early and mature aggregates (4 hours and 14 hours after addition of serum).

160   Indeed, we found that snail serum-induced aggregates were quantitatively less spherical than

161   those induced by FBS, as measured by the ratio of bounding box dimensions of each aggregate

162   (**Fig. 1I**). The difference was most noticeable in mature 14-hour aggregates. Regarding cell

163   density (measured by the intensity of cell fluorescence within the boundary of each aggregate),

164   snail serum-induced aggregates were initially similar to FBS-induced aggregates at 4 hours but

165   were less dense by 14 hours (**Fig. 1J**). Additionally, snail serum-induced aggregates were

166   rougher around the edges than those induced by FBS, causing a higher surface area to volume

167   ratio at both time points (**Fig. 1K**). Furthermore, snail serum-induced samples had more individual

168   cells not encompassed in aggregates than the FBS-induced samples. This difference was

169   significant at the 14-hour time point (**Fig. 1L**). Finally, while the snail serum-induced aggregates

170   were of similar height to FBS-induced aggregates at 4 hours, they ultimately reached greater

171   height than those induced by FBS at 14 hours (yet, this measurement was biased by especially

172   tall spires in the more asymmetric snail serum aggregates) (**Fig. 1M–O and Fig. S2A–D)**.

173   Interestingly, the morphological differences observed here under different chemical stimulation

174   mirror some of the morphological differences reported in mutant *Capsaspora* strains.[26,37]

175   Therefore, it is likely that multiple chemical and genetic factors contribute to the specific

176   multicellular structures formed by *Capsaspora* cell-cell adhesion.

177   In parallel, we also monitored the kinetics of cellular aggregation in response to snail serum

178   and compared it with aggregates induced using FBS. Although FBS-induced aggregates lasted

179   slightly longer than snail serum-induced aggregates, both persisted for over 20 hours. (**Fig. 2A–**

180   **B** and **Movie S1A–B**). We observed a small spike in aggregate size in the snail serum samples

181   at early time points. This was due to the initial formation of large, less circular aggregates, that

182   later divided into several smaller and rounder aggregates (**Fig. 2B–C**). This spike was not

183   observed in the FBS sample, because the aggregates became circular much more quickly.

184   Overall, snail serum and FBS induced similar—but not identical—aggregation morphology and

185   kinetics.

186   Together, these results suggest that serum-induced cellular aggregation is a relevant

187   response of *Capsaspora* to its host snail environment. We next sought to determine the specific

188   identity of the snail serum inducer(s).
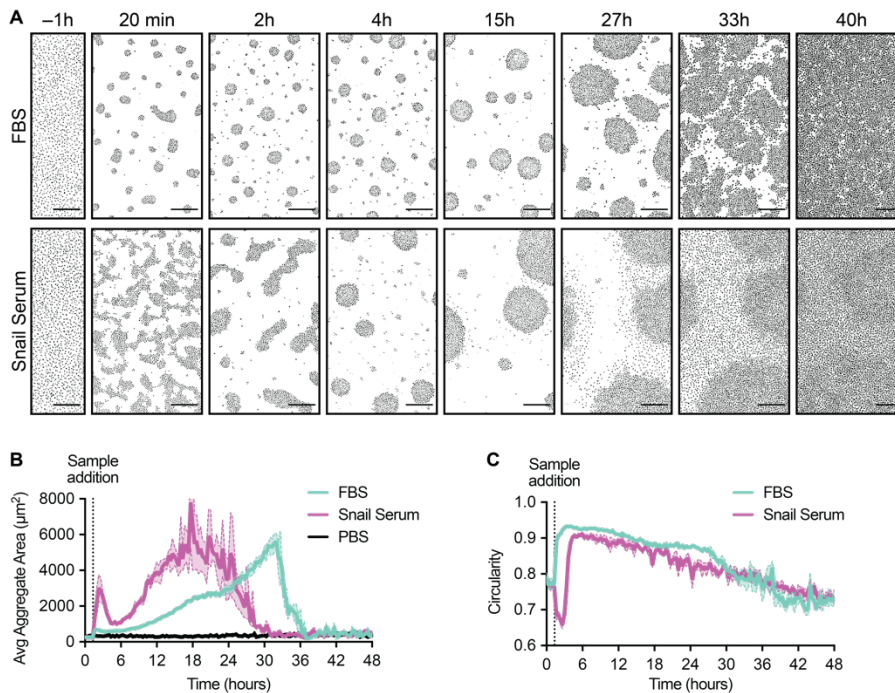
Figure 2: Dynamics of Capsaspora aggregates over time. (A) Representative images showing cellular aggregates monitored for 2 days after addition of 5% (v/v) FBS or 50% (v/v) >30 kDa snail serum components. Images were converted to binary in FIJI to enhance contrast. Scale bar is 250 μm. The full time-lapse is available as **Movie S1**. (B) The average aggregate areas measured every 20 minutes for 48 hours after addition of 5% (v/v) FBS or 50% (v/v) >30 kDa snail serum components. FBS-induced aggregates gradually increased in area over ~30 hours followed by a sudden disaggregation; however, snail serum induced an initial spike where aggregates were amorphous followed by the formation of circular aggregates that gradually enlarged and then gradually disaggregated. (C) Average circularity of aggregates calculated in two dimensions measured every 20 minutes for 48 hours after addition of 5% (v/v) FBS or 50% (v/v) >30 kDa snail serum components shows initial snail serum-induced aggregates were amorphous. Plots show means ± sem (n=3).

Lipids extracted from snail serum are sufficient to trigger aggregation

Because protein-free lipid particles were previously shown to induce aggregation,[27] we hypothesized that the macromolecular aggregation inducer(s) in snail serum were also lipid complexes. To test this hypothesis, we extracted the total lipids from snail serum and tested the

208 solubilized lipid extract for aggregation induction. Indeed, we found that the crude lipids induced

209 robust aggregation activity with an EC50 around 100 μg/mL (**Fig. 3A**). This concentration was

210 similar to the concentration of total lipids present in active dilutions of >30 kDa snail serum (see

211 **Materials and Methods** section), suggesting that lipids are sufficient to account for the

212 aggregation induction activity in >30 kDa snail serum.

213 We then physically and chemically characterized these emulsified crude serum lipid particles

214 that induced aggregation. First, we used transmission electron microscopy (TEM) to visualize

215 particle sizes (**Fig. 3B**) and dynamic light scattering (DLS) to determine the particle diameters.

216 The crude snail lipid particles were ~90 nm (**Fig. 3C**). This value is slightly more than three times

217 the diameter of low density lipoproteins (LDLs, which are the aggregation inducers in FBS).[27]

218 Next, we employed LC-MS to evaluate the chemical composition of the solubilized snail lipid

219 particles. Although analysis of crude snail serum extracts revealed the presence of over 800 lipids,

220 (see supplementary **Table S1 and Fig. S3**), the solubilized lipid particles did not contain the full

221 array of serum lipids (*i.e.*, some serum lipids resisted resuspension and were not delivered to the

222 cells). Nonetheless, a complex mixture of major lipid classes including diglycerides, wax esters,

223 triglycerides, and phospholipids was clearly incorporated into these aggregate-inducing particles

224 (**Fig. 3D** and **Fig. S3**). Therefore one (or many) lipids present in snail serum induce multicellular

225 aggregation of *Capsaspora*.

226 We then asked if the aggregation activity was due to a minor component or a major lipid

227 present in the extracted snail serum. First, to determine if a major lipid was responsible for the

228 activity, we prepared a simplified lipid mixture from representative lipids of each of the major lipid

229 classes present in the snail serum extract. The lipid mix, prepared from commercially available

230 synthetic lipids, contained glyceryl dioleate (DG), glyceryl trioleate (TG), dioleoyl

231 phosphatidylcholine (PC), 18:1/24:0 ceramide (Cer), and palmitoyl lysophosphatidylcholine

232 (LPC). Despite being a large class represented in the extracted lipids, we did not include wax

233 esters in this initial simple mix because we could not easily obtain short-tailed wax esters. We

234 combined the five aforementioned lipids at approximately their natural ratio in snail serum and

235 solubilized them by sonication into mixed-lipid particles. Remarkably, this simplified mixture

236 induced aggregation in a dose-dependent manner with similar potency to the crude snail lipids

237 (**Fig. 3E**). We also validated the formation of lipid particles by TEM and DLS measurements as

238 before, which revealed particles that were ~50 nm in diameter (**Fig. 3F–G**). We also determined

239 the final lipid ratio in the particles by LC-MS to be slightly different than the original intended ratio

240   (**Fig. 3H**), yet all lipids were incorporated into the soluble particles. Thus, a simple mixture of the

241   major snail serum lipids is sufficient to induce *Capsaspora* aggregation.

242   Then, to determine if a single lipid from snail serum was sufficient to induce aggregation, we

243   tested each component of the active lipid mix individually. We added each lipid to *Capsaspora* (at

244   the same concentration as in the simple lipid mix) and found pure dioleoyl PC (DOPC) lipids to

245   be active, while no other lipids elicited an aggregation response (**Fig. 3I**). The DOPC lipids

246   induced robust aggregation in a dose dependent manner with an EC50 of 20 µg/mL (**Fig. 3J**),

247   which is about five times more potent than the extracted natural lipids from snail serum and the

248   simplified lipid mix. We also validated the formation of lipid vesicles of ~40 nm diameter with TEM

249   and DLS (**Fig. 3K–L**). Moreover, to determine if 20 µg/mL is a biologically relevant concentration,

250   we quantified the amount of DOPC in snail serum using LC-MS. Based on spectral intensity

251   normalized to an internal PC control, we estimated the concentration of DOPC in snail serum to

252   be about 2 µg/mL (~10X lower than the EC50 of pure DOPC vesicles). Therefore, DOPC is likely

253   not the sole inducer of aggregation present in snail serum (*e.g.* other PCs in snail serum may

254   contribute as well). In summary, pure DOPC, a lipid present in snail serum, is sufficient to induce

255   *Capsaspora* multicellular aggregation; however, it is likely that other lipids also contribute to the

256   phenotype.

257

258
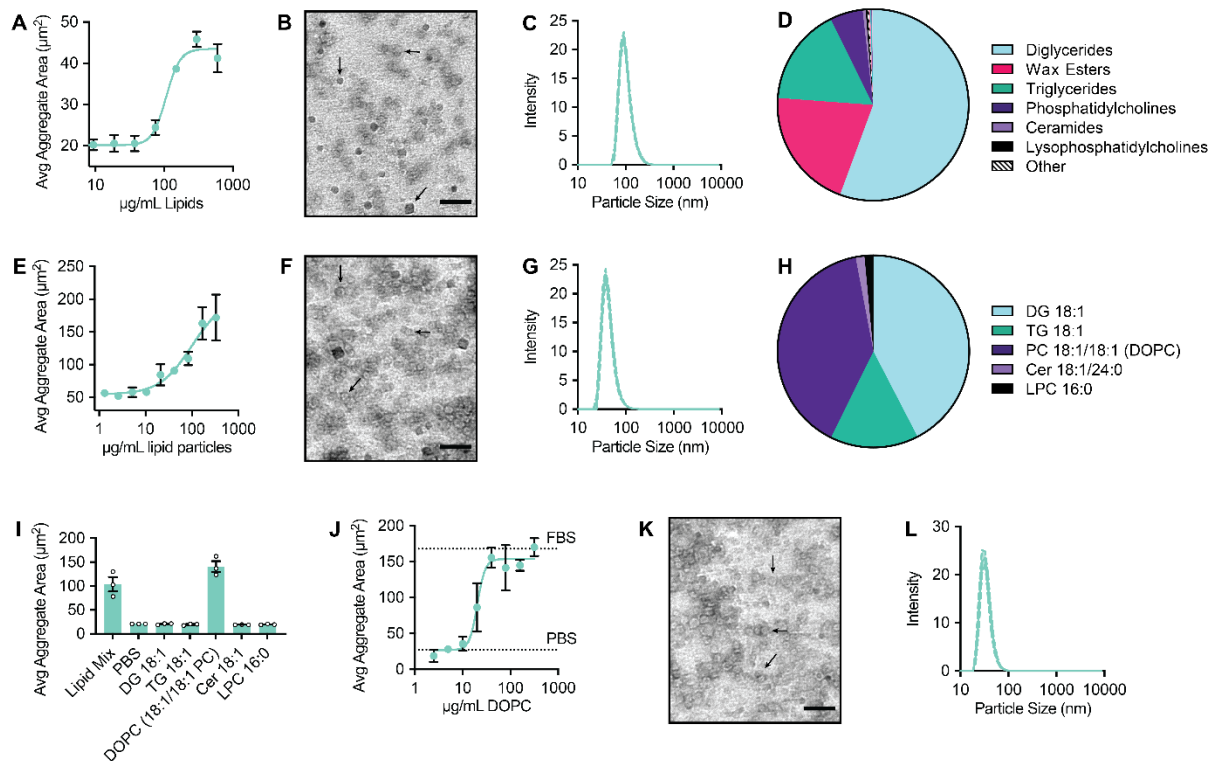
Figure 3. Lipids isolated from *Biomphalaria* snail serum induce aggregation. (A) Average area of aggregates induced by a dilution series of lipids isolated from snail serum and prepared into soluble emulsions. Area plotted as a function of lipid concentration in µg/mL. Lipids induced aggregation in a dose-dependent manner with an EC50 = 100 µg/mL. (B) Representative TEM image of prepared crude snail serum lipid particles show active lipids were incorporated into particles with a range of sizes. (C) Crude snail serum lipid particles were ~90 nm in diameter as measured by DLS. (D) Pie chart of the major lipid classes present in the prepared and tested crude snail serum lipid particles. The most abundant lipid classes were diglycerides, wax esters, triglycerides, and phosphatidylcholines. (E) Average area of aggregates induced by a simple mixture of synthetic lipids. The simple mix contained glyceryl dioleate (DG), glyceryl trioleate (TG), dioleoyl phosphatidylcholine (PC), 18:1/24:0 ceramide (Cer), and palmitoyl lysophosphatidylcholine (LPC). Lipids significantly induced aggregation at concentrations ~100 µg/mL, similarly to the extracted lipids. (F) Representative TEM image of particles prepared using the simple synthetic lipid mix showed a range of sizes, much like the natural lipid preparation. (G) Synthetic lipid mixture particles were ~50 nm in diameter as measured by DLS. (H) Pie chart of the final lipid ratios included in the soluble synthetic lipid particles. (I) Average area of aggregates induced by either the simple lipid mix or the individual lipids tested at the same concentration as present in the simple lipid mix. Of the individual lipids, only DOPC induced aggregation. (J) Average area of aggregates induced by pure DOPC lipid vesicles. DOPC induced aggregation in a dose-dependent manner (EC50 = 20 µg/mL). (K) Representative TEM image of DOPC vesicles. (L) DOPC vesicles were ~40 nm in diameter as measured by DLS. For plots, means ± sem (n=3) are shown, and values from individual replicates are displayed with small circles. For microscopy images, scale bars are 100 nm, arrows highlight example particles.

Since the morphologies of FBS- and snail serum-induced aggregates had differed, we next assessed the morphology of DOPC-induced aggregates using the same quantifiable features measured in **Fig. 1**. We found that DOPC-induced aggregates generally resembled those induced by FBS and/or snail serum and that their morphology depended some on the concentration of DOPC (**Fig. 4A–K**). At intermediate DOPC concentrations, the DOPC-induced aggregates were similar in sphericity, cell density, and smoothness to snail serum-induced aggregates (**Fig. 4B– D, G–I, L–N**). However, more cells remained outside of aggregates in the DOPC-induced condition than those induced by either FBS or snail serum (**Fig. 4E, J, O**). The DOPC-induced aggregates were similar in height to FBS-induced aggregates (**Fig. 4F, K, P**). Overall, most

11

292   morphological features of DOPC-induced aggregates were similar to those induced by snail

293   serum or FBS. The dependence of morphology on the identity and concentration of lipids

294   suggested that *Capsaspora* aggregation morphology may differ depending on the exact

295   hemolymph composition of its host.

296   Finally, we also monitored the aggregation dynamics induced by DOPC over time. We found

297   that the dynamics of DOPC-induced aggregation were similar to the case of snail serum induction,

298   although they formed quicker and dissipated earlier (**Fig. 4Q** [top right panel] and **Movie S2**).

299

300

12
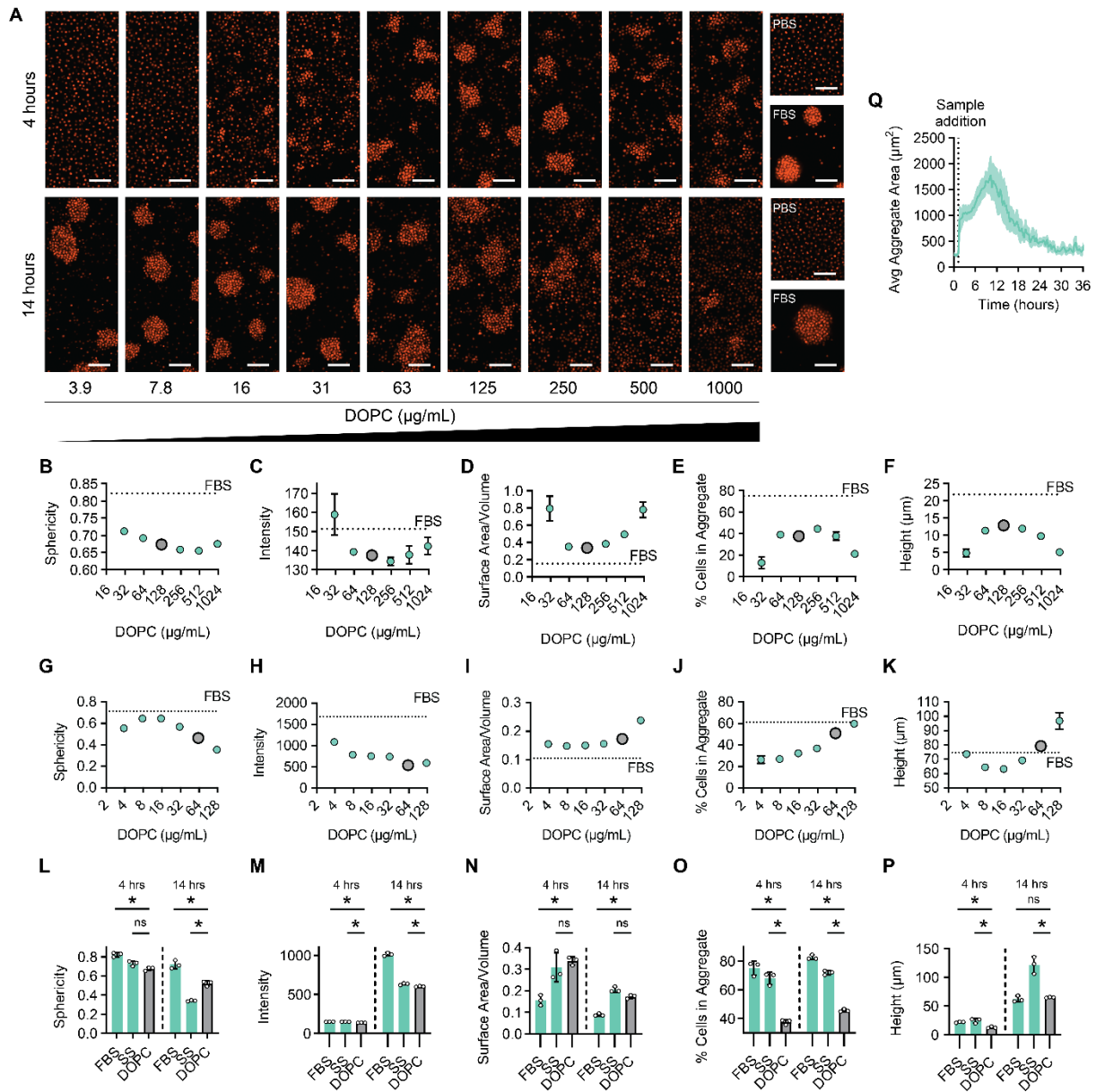
Figure 4. *Capsaspora* aggregate morphology is sensitive to the nature of the inducer, concentration of the inducer, and time. (A) Representative confocal microscopy images of tdTomato-expressing *Capsaspora* cell aggregates after 4 hours and 14 hours of induction with increasing concentrations of DOPC. Scale bars are 50 μm. (B–F) Plots of morphology features of aggregates after 4 hours of induction with increasing concentrations of DOPC. The dotted line represents the value for FBS-induced aggregates, and the larger grey circle is the concentration used in L–P (125 μg/mL for 4 hours). (G–K) Plots of morphology features of aggregates after 14 hours of induction with increasing concentrations of DOPC. The dotted line represents the value for FBS-induced aggregates, and the larger grey circle is the same concentration used in L–P (63 μg/mL for 14 hours). (B/G) Sphericity of aggregates as determined by the ratio of aggregate bounding box dimensions. The sphericity of aggregates generally decreased with increasing concentration of DOPC. (C/H) The density of aggregates induced by DOPC as calculated by the average intensity of fluorescence. The density generally decreased with increasing DOPC concentration. (D/I) The roughness of the aggregate surface calculated by the surface area to volume ratio. The roughness of aggregates increased at the highest concentrations of DOPC. (E/J) The percentage of cells included in an aggregate compared to the total number of cells in the image positively correlated with the concentration of DOPC at 14 hours, but exhibited a non-monotonic dose response at 4 hours. (F/K) The height of aggregates measured by analysis of confocal microscopy images in three dimensions. At 14 hours, height positively correlated with the concentration of DOPC, but again a non-monotonic dose response was observed at 4 hours. (L–P) Plots of morphology features of aggregates after 4 hours and 14 hours of induction with either 5% (v/v) FBS, 50% (v/v) snail serum, or DOPC (125 μg/mL at 4 hours or 62 μg/mL at 14 hours). The data in panels L–P and the data in panels B–K were collected in separate experiments on separate days. (L) The sphericity of DOPC-induced aggregates was similar to FBS- and snail serum-induced aggregates at 4 hours and lied between those at 14 hours. (M) Density of DOPC-induced aggregates were slightly less than snail serum-induced aggregates at both time points. (N) DOPC-induced aggregates were similar in roughness to snail serum-induced aggregates, both of which were rougher than FBS-induced aggregates at both time points. (O) There were significantly more non-aggregated cells present in DOPC-induced aggregate images than in either serum-induced sample at both time points. (P) DOPC-induced aggregates were similar in height to FBS-induced aggregates and shorter than those induced by snail serum. (Q panel in top-right) The average aggregate area monitored every 20 minutes for 36 hours after induction by 62.5 μg/mL of DOPC vesicles over time. For plots, means ± sem (n=3) are shown, and values from individual replicates are displayed with small circles.

335

## *Capsaspora* responds to host infection with *Schistosoma mansoni*

337   Since aggregation was sensitive to the concentration of lipid inducers, we hypothesized that

338 *Capsaspora* could sense physiological changes in its host snail that alter serum lipid levels. If so,

339 its aggregation may be an adaptive response to these changes in its host physiology. Some lipids

340 present in *Biomphalaria* serum are known to change in response to the snail's metabolic state.

341 For example, snails fed different diets have exhibited different serum levels of triglycerides and

342 other neutral lipids.[38,39] Furthermore, infection with parasites can alter lipid levels in *Biomphalaria*

343 snails. For instance, serum cholesterol and triglyceride levels decrease in *B. glabrata* in response

344 to infection with *Echinostoma paraensei*.[40] Triglycerides in the entire snail body also drop in

345 response to infection with *Echinostoma caproni*.[41] Particularly of interest for our DOPC-induced

346 aggregation, whole-snail PCs have been shown to double after 8 weeks of infection by *E.*

347 *caproni*.[41] Therefore, to test if *Capsaspora* could sense schistosome-induced differences in host

348 serum lipid composition, we harvested serum from naïve outbred M-line *B. glabrata* snails as well

349 as identical M-line snails that had been infected with 10 PR1 (Puerto Rico Strain 1) *Schistosoma*

350 *mansoni* miracidia (and were shedding mature schistosome cercaria). We tested the two sera for

351 *Capsaspora* aggregation induction and observed a substantial difference between them (**Fig. 5A**).

352 Remarkably, serum from infected M-line snails induced *much greater aggregation* than the naïve

353 M-line snails, which showed comparatively little aggregation activity (**Fig. 5A–B**). Moreover, the

354 aggregation induced by serum from infected M-line snails was dose-dependent (**Fig. 5C**).

355   To explain the difference, we hypothesized that the infected snail serum contained higher

356 levels of DOPC and/or other phosphatidylcholines (PCs). Thus, we analyzed the lipid contents of

357 each sample using LC-MS/MS. Of the 800 lipids detected, we found 104 to be significantly

358 different between the infected and naïve snail sera (**Fig. 5D, Table S1**). Triglycerides and

359 diglycerides generally decreased upon *S. mansoni* infection, which is consistent with previous

360 studies of echinostome infections.[40,41] Also consistent with previous work of echinostome-infected

361 snails,[41] *many of the PC lipids were significantly higher in the infected samples* (**Fig. 5D**), *including*

362 *DOPC* (**Fig. 5E**). Furthermore, not a single detected PC was significantly depleted in the infected

363 sample. Some abundant PCs were not substantially different between the two samples, rendering

364 the sum of all PCs insignificantly different by a t-test (**Fig. 5F**). However, since several individual

365 PCs were increased in the infected snails, it is plausible that the increased concentrations of a

366 certain class of PCs in the infected snail serum caused the improved aggregation. Overall, these

367 data show that *Capsaspora's* aggregation phenotype is sensitive to schistosome-induced

368   changes in host serum and that *Capsaspora* aggregation correlates with the serum concentration

369   of DOPC and many other PCs.

370
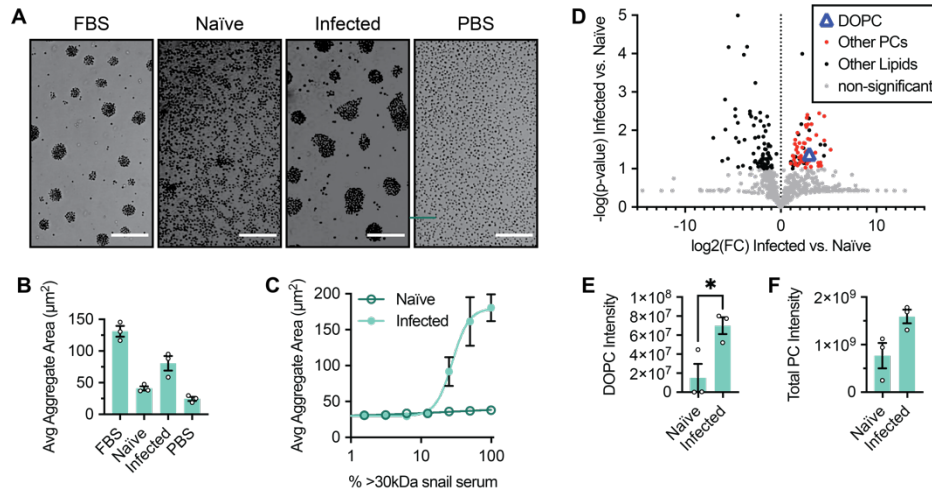
371

372   **Figure 5: *Capsaspora* aggregates differently in response to serum from snails infected with**

373   **schistosomes.** (A) Representative images of *Capsaspora* cell aggregates induced by either 5%

374   (v/v) FBS, 50% (v/v) >30 kDa serum from naïve M-line snails, 50% (v/v) >30 kDa serum from

375   schistosome-infected M-line snails, or 5% (v/v) PBS control. Scale bars represent 100 μm. (B)

376   Average aggregate area of *Capsaspora* cells induced by snail serum samples compared to FBS

377   and PBS controls. (C) Dose response curve of average aggregate area of cells induced by naïve

378   and infected sera. Infected serum induced aggregation significantly better than naïve snail serum.

379   (D) Volcano plot showing the fold-change (FC) of individual lipids in naïve vs. infected serum,

380   detected by LC-MS/MS. The p-values were calculated from analysis of 3 distinct batches of snails

381   in each condition. Many PCs showed significant increases in the infected snails (see SI for the

382   full table of lipids). (E) Comparison of DOPC $[M+H]^+$ intensity in each sample (student's t-test

383   p=0.03). (F) Comparison of total identified PC $[M+H]^+$ intensity summed in each sample (student's

384   t-test p=0.05). For plots B, C, E, and F, means ± sem (n=3) are shown, and values from individual

385   replicates are displayed with small circles.

386

387   ***Capsaspora* responds differently to serum of different *Biomphalaria***

388   ***glabrata* strains**

15

Unexpectedly, we observed that the naïve M-line snail serum above failed to induce robust aggregation at any tested concentration (**Fig. 5C**). This finding contrasted the previous results using serum from naïve NMRI snails, which repeatedly induced robust aggregates (**Fig. 1E–G**). Moreover, this *Capsaspora* aggregation difference between M-line and NMRI snail sera persisted upon repeated inspection (**Fig 6A–B**). This difference could be due to the genotypes of the snails, or it could be due to snail age or different snail husbandry conditions (*e.g.,* temperature, food, or snail density in tanks, see **Materials and Methods** section). To explain the different aggregation potencies of the sera, we hypothesized that they might contain different levels of phosphatidylcholine lipids. Specifically, the NMRI snail serum may have contained higher concentrations of PCs. Thus, we quantified the lipid content of serum from naïve M-line and NMRI snail strains by LC-MS/MS analysis. The two naïve snail sera did not contain significantly different DOPC concentrations (**Fig. 6C–D**). However, several other PCs were significantly higher in the NMRI serum compared to the M-line serum, and no PCs were lower in the NMRI serum (**Fig. 6C**). Although the sum of PCs was insignificantly different between the samples (**Fig. 6E**), it is plausible that a subset of specific PCs is responsible for the observed difference in aggregation induction by our NMRI and M-line snails. Alternatively, we explored other explanations below.

We hypothesized that different *proteins* in the sera might also account for the different aggregation induction of the two naïve sera. Two scenarios are possible: 1) inhibitory protein(s) that interfere with aggregation are lower in the NMRI serum, or 2) activator protein(s) present in the NMRI snails are needed for robust aggregation. To test these possibilities, we performed proteomics analysis of the two snail strains and found 18 proteins significantly higher in M-line serum and 23 proteins significantly higher in the NMRI serum (**Fig. 6F, Table S2**). Two members of the serpin superfamily of serine protease inhibitors were significantly higher in the NMRI serum, suggesting that proteases might inhibit aggregation and these protease inhibitors curtail that inhibition. Additionally, several fibrinogen-related proteins (FREPs) and a couple C-type lectins were differentially abundant in the two snail sera. A FREP immune protein or lectin could bind to *Capsaspora* (or the lipid inducer itself) and block aggregation. Alternatively, one of these proteins may activate *Capsaspora* by somehow priming the cells to aggregate. Interestingly, subsequent proteomics analysis of the *infected* M-line snail serum also showed one FREP and one C-type lectin at levels similarly low to their levels in NMRI serum, demonstrating multiple inverse correlations between these specific proteins and aggregation induction activity (**Fig. S4, Table S2**).

421   Further work is needed to confidently conclude if the PC differences are sufficient to explain

422   the aggregation induction differences across host snail sera (or if other serum components inhibit

423   or promote aggregation). Also, further work will determine if the differential aggregation induction

424   is due to genomic differences between NMRI and M-line snails or environmental differences in

425   snail husbandry. Nevertheless, these data clearly show that *Capsaspora* can recognize other host

426   differences beyond infection with schistosomes.

427
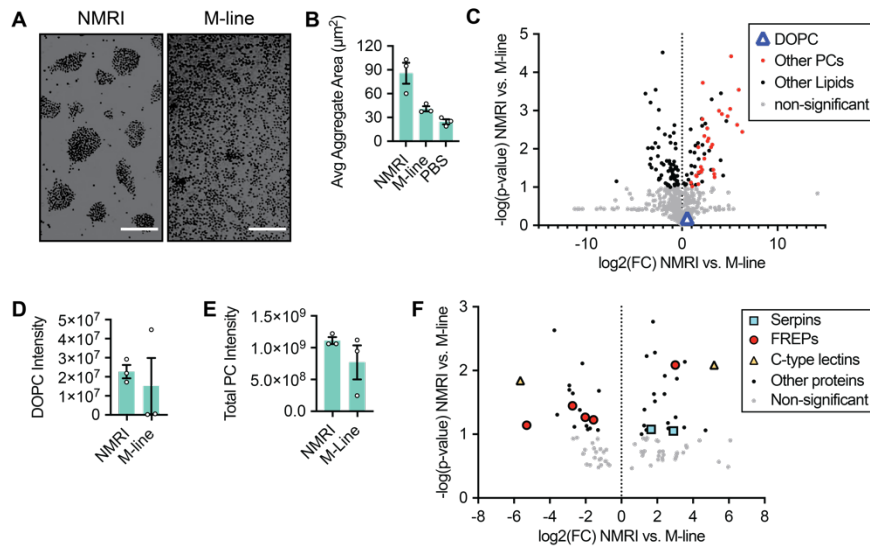
428

429   **Figure 6: The *Capsaspora* aggregation phenotype discriminates between snail strains.** (A)

430   Representative images of *Capsaspora* aggregates induced by 50% (v/v) >30 kDa snail serum

431   from naïve NMRI snails and M-line snails. Scale bars represent 100 μm. (B) Average area of

432   *Capsaspora* aggregates showed that naïve NMRI snail serum is much more active than naïve M-

433   line serum. (C) Volcano plot of the lipids identified by LC-MS/MS analysis of snail serum samples.

434   Many PCs were higher in the active NMRI serum, but DOPC was not significantly different. (D)

435   Comparison of DOPC [M+H]$^+$ intensity in each sample (insignificant change by student's t-test).

436   (E) Comparison of total identified PC [M+H]$^+$ intensity summed in each sample (student's t-test

437   p=0.2). (F) Volcano plot showing fold-change (FC) of individual proteins in naïve NMRI vs. M-line

438   snail sera determined by LC-MS/MS of tryptic peptides. The p-values were calculated from

439   analysis of 3 distinct batches of snails in each condition. 18 proteins were significantly higher in

440   M-line than in NMRI and 23 proteins were significantly lower in M-line than NMRI. Notably, two

441   serpins, five FREPs, and two C-type lectins were significantly different. For plots B, D, and E,

442   means ± sem (n=3) are shown, and values from individual replicates are displayed with small

443   circles.

444

DISCUSSION

446 We have discovered that *Capsaspora* (a predator of parasitic schistosomes) can sense and
447 respond to a specific chemical factor within its host snail's hemolymph. Namely, *Capsaspora*
448 aggregates in response to a snail serum phosphatidylcholine (PC) (**Fig. 7A–B**). This discovery is
449 the first example of a physiological response of *Capsaspora* to its host, which may inform how it
450 colonizes its host and could therein exclude schistosome parasites.

451

452 NMRI snail   NMRI snail   M-line snail   M-line snail + schistosomes
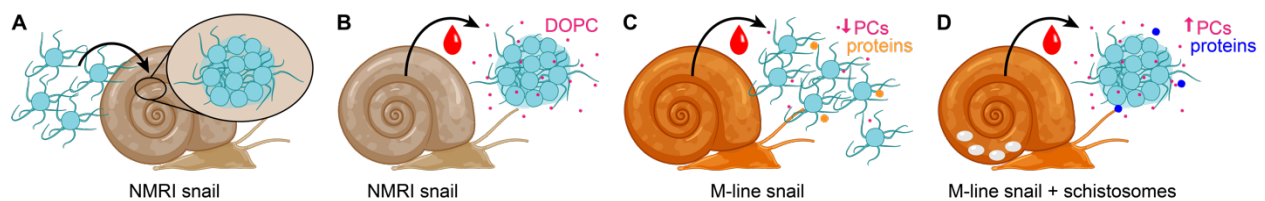
453 **Figure 7: Overview of *Capsaspora* aggregative response to host and upon distinct host-**
454 **pathogen interactions.** (A) When introduced to NMRI snail tissue, *Capsaspora* aggregates. (B)
455 NMRI snail serum also induces *Capsaspora* aggregation, and the serum lipids are responsible
456 for the aggregation—particularly dioleoyl phosphatidylcholine (DOPC). (C–D) M-line snail serum
457 fails to induce robust *Capsaspora* aggregates *in vitro* unless the snails have been pre-infected
458 with schistosomes. Schistosome infection increases the concentration of DOPC (and other PCs)
459 and alters the serum proteome.

460

461 *Capsaspora* was recently shown to aggregate in response to FBS *in vitro*.[27] However,
462 mammalian serum is irrelevant to the expected natural life of *Capsaspora*, which has only been
463 detected in *Biomphalaria* snails and once in fish feces (possibly caused by the fish eating snails).[42]
464 Thus, our discovery that *Biomphalaria* tissue and hemolymph induce aggregation suggests that
465 this aggregative phenotype *is an ecologically relevant response to a host environment*. As further
466 support for the ecological significance of this phenotype, we found that all three existing isolated
467 strains of *Capsaspora* aggregate in response to snail hemolymph—suggesting that *Capsaspora*
468 aggregation is a widely conserved cellular response to the host environment.

469 We furthermore identified a single pure lipid from the snail hemolymph that is sufficient to
470 induce aggregation: dioleoyl phosphatidylcholine (DOPC). Since phosphatidylcholines are major
471 components of LDLs, this finding is consistent with our earlier work, which revealed that a

472   combination of LDL lipids collectively induced aggregation.[27] Quantification of DOPC in snail

473   serum revealed that its concentration is below the threshold level required for pure DOPC vesicles

474   to quickly induce aggregation. Therefore, it is likely that other components in snail serum promote

475   aggregation, as well. For example, other phosphatidylcholines may also induce aggregation—we

476   are currently assessing the aggregation induction ability of a wide panel of phospholipids.

477   Additionally, other serum components may synergize with DOPC to increase its potency. In fact,

478   the aggregate morphologies upon DOPC induction differed some from those induced with whole

479   snail serum (or with FBS), which also suggests that additional serum components contribute to

480   aggregate formation. Since some *Capsaspora* mutants have exhibited similar differences in

481   aggregation morphology, the unknown serum components may interact with these newly

482   characterized pathways in *Capsaspora* to modify aggregate structure.[37]

483   Having identified the molecular cue of aggregation induction in snail serum, we asked whether

484   *Capsaspora* would be able to use this cue to sense changes in the physiological state of its snail

485   host. Other work has shown that certain lipid classes exhibit different abundance in snails under

486   starvation and infection.[38-41] Remarkably, we found that schistosome-infected snails harbored

487   elevated concentrations of DOPC (the aggregation inducer), and correspondingly, this serum

488   more potently induced *Capsaspora* aggregation (**Fig 7C–D**). Therefore, it appears that

489   *Capsaspora* can sense the infected state of its host snail and responds with more robust

490   aggregation.

491   Furthermore, we discovered that *Capsaspora* can differentiate between different inbred

492   strains of snails grown under different laboratory conditions. It aggregated far better in uninfected

493   NMRI snail serum than in uninfected M-line serum. Surprisingly, we found no significant difference

494   in the concentrations of DOPC between the two snail strains. However, other PCs were

495   significantly higher in NMRI serum (and none were higher in M-line serum). Therefore, the

496   induction ability may still rely on a threshold concentration of certain PCs. Alternatively,

497   aggregation may be induced or inhibited by other factors that differ between the strains. The

498   serum proteomes of the two snail strains revealed different levels of FREPs. These proteins serve

499   as immune effectors in snails[43] and are known to differ in expression across inbred lines[44] and

500   during infections.[45] M-line snails may produce specific FREPs that block *Capsaspora* aggregation

501   by preventing its interaction with DOPC or by directly inhibiting its cell-cell contacts. If this

502   hypothesis proves true, it is notable that some FREPs were also depleted in the infected M-line

503   serum, including one that was depleted in the active NMRI serum. Therefore, the increased

504   aggregation in infected serum could be *both* due to increased DOPC concentrations *and*

505 decreased concentrations of certain FREPs. Alternatively, the NMRI FREPs may play a role in

506 promoting DOPC-induced aggregation.[46] Serpin protease inhibitors, a class of proteins that have

507 previously been investigated for their role in host-pathogen interactions,[47] were also increased in

508 the aggregation-inducing NMRI serum, possibly indicating an anti-aggregation effect by

509 proteases. Ultimately, the chemical composition of sera from different snail strains grown in

510 different laboratory conditions yielded remarkably different *Capsaspora* aggregation, indicating a

511 means of distinguishing between potential hosts.

512 In total, these discoveries raise the question of why *Capsaspora* aggregates inside its snail

513 host. Furthermore, it is curious what benefit *Capsaspora* would gain from aggregating more in

514 schistosome-infected snails than in naïve snails. The potential benefits of multicellular forms are

515 myriad,[48-50] but we mention a few specifically here. First, diverse microbes form multicellular

516 adhesive phenotypes to remain in a favorable environment.[48-50] For *Capsaspora*, the large

517 aggregates may localize to certain favorable tissues or avoid excretion from the host. A second

518 potential benefit is efficient utilization of secreted exoenzymes. Like many osmotrophic microbes,

519 *Capsaspora* is believed to secrete enzymes to liberate soluble nutrients.[28] As more cells co-

520 localize, they benefit from each other's "common goods" and feed more efficiently. This logic has

521 explained the frequent exoenzyme regulation by quorum sensing (or "diffusion sensing") in

522 bacteria.[51] Finally, aggregation may protect *Capsaspora* from the snail immune system.

523 Multicellular growth is known to protect symbiotic and free-living microbes from predation.[52-55]

524 Because snail hemolymph contains immune cells (hemocytes) that can engulf prey[56] as well as

525 release toxic soluble factors,[57,58] *Capsaspora* aggregation may afford protection from these

526 insults. Why *Capsaspora* would particularly benefit from aggregation in schistosome-infected

527 snails is also unclear. Perhaps the elevated PC levels indicate a more nutrient-rich environment

528 that favors adhesion and cooperative feeding. Alternatively, higher PC concentrations may

529 indicate an elevated immune state that necessitates protective aggregation.

530 It is tempting to speculate that the different aggregation responses to sera from different snails

531 will lead to different abilities of *Capsaspora* to colonize those snails. Because serum-induced

532 aggregation is conserved across all existing isolates of *Capsaspora*, the phenotype is likely

533 important for its natural fitness in the snail. However, further work is necessary to determine the

534 necessity of aggregation for snail colonization. If aggregation indeed promotes colonization, then

535 *Capsaspora* may fare better in schistosome-infected snails and in NMRI snails than in uninfected

536 M-line snails. In ongoing work, we are testing this hypothesized dependence of *Capsaspora*

537 colonization on snail strain and infected status.

538   Lastly, aside from its symbiosis with snails, *Capsaspora* is also an important model for

539   studying the evolution of multicellular phenotypes in animals.[23] It is one of the closest living

540   relatives of animals and contains many genes that are important for cell-cell adhesion and

541   signaling in animals.[59] Furthermore, Ruiz-Trillo and co-workers have proposed that *Capsaspora*-

542   like aggregation in the unicellular ancestor of animals may have been a pivotal step in the

543   evolution of the first multicellular animals.[60] Specifically, cell aggregation may have been the first

544   step to establish obligate multicellular animals (instead of, or in addition to, incomplete separation

545   of cells after clonal cell division). Therefore, dissecting how and why aggregation occurs in

546   *Capsaspora* may illuminate potential mechanisms of aggregative multicellularity in the unicellular

547   ancestor of animals and in the earliest animals. Now that a pure chemical inducer is known, it can

548   be leveraged into biochemical and genetic experiments to determine how *Capsaspora* regulates

549   its multicellularity, both *in vivo* and *in vitro*. Comparative genomics of the regulatory pathway(s)

550   across animals and non-animal holozoans can then assess the potential ancestry of regulated

551   cell-cell adhesion phenotypes in animals. Along this line, it will also be informative to determine if

552   *Capsaspora*'s relatives (*e.g., Pigoraptor* spp.[61], *Ministeria vibrans*[62], *Txikispora philomaios*[63], and

553   *Tunicaraptor unikontum*[64], see **Fig. S5**) also aggregate in response to PCs, especially given that

554   they exhibit free-living or parasitic distinct lifestyles. If so, this response to PCs may be ancestral,

555   predating *Capsaspora*'s symbiosis with snails and perhaps even predating the divergence of

556   animals from their unicellular holozoan ancestor. Overall, by more deeply elucidating the

557   mechanism of this lipid-induced aggregative response and the breadth of its conservation across

558   phyla, we (and others) can discern the significance of lipids in regulating multicellular behaviors

559   in the evolution of animals.

560

CONCLUSION

561

562   In sum, we discovered that a snail symbiont that is capable of killing human parasites can

563   adapt its behavior to its host snail environment. Namely, the symbiont *Capsaspora* forms

564   multicellular aggregates in *B. glabrata* snail host tissue and hemolymph. *Capsaspora* senses at

565   least one specific lipid (DOPC) from its host serum and likely uses the concentration of this lipid

566   and its analogs to sense the physiological state and genotype of its host. Because this response

567   is conserved across several symbiont isolates, it is likely significant for the natural life of

568   *Capsaspora*. These findings pave the way for further work to investigate the persistence of

569   *Capsaspora* within the host, the importance of *Capsaspora* aggregation for its ability to colonize

570 snails, and ultimately, this symbiont's ability to limit the proliferation and spread of parasitic

571 schistosomes from snails.

572

573 ACKNOWLEDGMENTS

592

593

594 AUTHOR CONTRIBUTIONS

595 Conceptualization, R.Q.K., N.R.R., J.P.G.; Methodology, R.Q.K., M.R.L, C.G., J.P.G.;

596 Investigation, R.Q.K., E.B.G., M.R.L., M.C.S., C.G., L.P.B.; Writing – Original Draft, R.Q.K.,

597 J.P.G.; Writing – Review & Editing, R.Q.K., M.R.L., N.R.R., J.P.G.; Visualization – R.Q.K., J.P.G.;

598 Supervision, J.P.G.; Funding Acquisition, J.P.G.

599

600 DECLARATION OF INTERESTS

601 The authors declare no competing interests.

602

603

MATERIALS AND METHODS

Cell strain and growth conditions

Capsaspora owczarzaki cell cultures (strain ATCC®30864) were grown axenically in 25 cm^2 culture flasks with 6 mL ATCC media 1034 (modified PYNFH medium) containing 10% (v/v) heat-inactivated Fetal Bovine Serum (FBS), hereafter *growth media*, in a 23°C incubator. Adherent stage cells (filopodiated amoebae) at the exponential growth phase were obtained by passaging ~100–150 µL of adherent cells at ~90% confluence in 6 mL of growth media and grown for 24–48 hours at 23ºC until ~100% confluent.

M-line *Capsaspora owczarzaki* cell cultures (strain ATCC®50973) were grown axenically in 25 cm^2 culture flasks with 6 mL *growth media*, in a 23°C incubator. Cells were maintained by passaging ~1 mL of adherent cells at ~1x10^6 cells/mL in 5 mL of growth media and grown for 1 week at 23ºC until ~100% confluent.

Salvador *Capsaspora owczarzaki* cell cultures (strain ATCC®50974) were grown axenically in 25 cm^2 culture flasks with 6 mL *growth media*, in a 23°C incubator. Cells were maintained by passaging ~3 mL of adherent cells at ~2.8x10^6 cells/mL in 3 mL of growth media and grown for 1 week at 23ºC until ~100% confluent.

Snail rearing and maintenance conditions

Biomphalaria glabrata NMRI snails were obtained from the Biomedical Research Institute (Rockville, MD) (BRI) Schistosomiasis Resource Center. Snails were kept in tanks with about 5 L of artificial pond water (BRI protocol: 0.46 µM $FeCl_3$, 220 µM $CaCl_2$, 100 µM $MgSO_4$, 310 µM KH_2PO_4, 14 µM $(NH_4)_2SO_4$ in water adjusted to pH 7.2 with NaOH) with no more than 50 snails per tank until experiments were conducted. Snails were fed romaine lettuce once per week or earlier if they ran out unless otherwise stated. Pond water was changed once per week, or sooner if water was cloudy, by transferring all snails into a new tank with fresh artificial pond water.

Biomphalaria glabrata outbred M-line snails were maintained in plastic 20 L tanks filled with 15 L of artificial pond water with no more than 30 snails per tank. Snails were fed red leaf lettuce and 2 Wardly® shrimp pellets 2 times a week. The water was changed once per month. Snails were maintained between 25-27ºC on a 12h:12h light-dark cycle.

Harvesting snail serum

Serum was harvested from snails measuring between 10 and 30 mm. Snails were removed from their growth tanks, rinsed with autoclaved water, and dried with paper towels or KimWipes. Serum was harvested by the headfoot retraction method.[65] Briefly, using 200 μL micropipettes or 1 mL glass pipettes, the tip was tapped gently onto the snail headfoot, causing it to retract and hemolymph to pour out from the hemal pore. As the foot retracted, serum was collected into the pipette tip and transferred to microcentrifuge tubes. After harvesting all possible serum, snails were placed in stage 1 of a 2-stage euthanasia solution[66] (95% (v/v) water + 5% (v/v) ethanol) for ten minutes, and then transferred to stage 2 (95% (v/v) ethanol + 5% (v/v) water) for five minutes. Tubes containing snail serum were centrifuged at 14,000xg for 15 minutes to move any mucus collected to the top of the tube. Bright red, transparent serum was collected from the bottom of the tube and diluted 1:1 in Chernin's balanced salt solution (CBSS+)[67] before sterile filtering through at 0.22 μm filter. Sterile serum was stored at 4°C until use.

General aggregation assay methods

All aggregation assays were performed at room temperature. Brightfield imaging was performed using the following instruments: Leica DMi1 inverted microscope with an MC120 HD camera, Leica DMIL inverted microscope with Flexacam C3 camera, an Olympus OSR spinning disk confocal microscope with a Hammamatsu Flash 4 V2 camera, and an Incucyte S3 Live-Cell Analysis System. Depending on well size and microscope used, each well was imaged at up to 3 distinct locations using 5X or 10X magnification. Average aggregate areas were typically measured by batch processing with a standard macro script in Fiji Imaging Software[27,68] (see *Image analysis* below).

Aggregation assay on ultra-low attachment plates

Two days before the assay, 100% confluent adherent cells growing in 25 cm^2 culture flasks were given fresh growth media (termed the "feed step"). One day before the assay, cells were washed and resuspended in FBS-free assay media and allowed to sit overnight (termed the "starve step"). After starvation, the day of the assay, $8*10^5$ cells were seeded in 180 μL of FBS-free media per well in a 96-well ultra-low attachment microplate (#CLS3474, Corning) and allowed to settle for 2

24

664   hours. Putative aggregation inducers were added such that the total volume in a well was 200 µL.

665   Typically, aggregates were assessed by microscopy after 90 min.

666

667   **Image analysis for aggregation assays**

668   Average aggregate areas were typically measured by batch processing with a standard macro

669   script in Fiji Imaging Software version 2.1.0/1.53c.[27,68] Briefly, the macro steps included: set the

670   scale of the image appropriate for the microscope conditions, convert the image to binary, analyze

671   particles (size 0-infinity), export results to clipboard. A copy of the FIJI macro is available upon

672   request.

673

674   ## *Capsaspora* forms multicellular aggregates in snail tissue

675   **Generating a *Capsaspora* line stably expressing tdTomato (related to Fig. 1C–D, I–M, and**

676   **Fig. 4A–P)**

677   A tdTomato expression plasmid was generated from plasmid pJP72.[26] The tdTomato gene was

678   synthesized by GenScript with codons optimized for *Capsaspora*. The gene was cloned into

679   pJP72, replacing the mScarlet protein-coding region. The resulting plasmid (pJG01) is available

680   from Addgene (#213505), and its sequence is deposited there (www.addgene.org). *Capsaspora*

681   cells were transfected following the protocol by Phillips et. al (2022).[26] Briefly, on the first day,

682     $3*10^5$ cells in exponential growth phase were seeded in 800 µL onto sterile 12 mm circular glass

683   coverslips in a well of a 24-well plate and allowed to settle overnight. On the second day, the

684   growth medium was removed and replaced with transfection medium (Scheider's Drosophila

685   Medium with 10% (v/v) FBS, supplemented with 25 µg/mL ampicillin) and allowed to incubate for

686   10 minutes. Two samples each were treated with Opti-MEM with 2 µg of transfection DNA (either

687   pJG01, or negative control without DNA) along with TransIT-X2 transfection reagent (Mirus Bio)

688   premixed and allowed to incubate 5 minutes at room temperature. Cells were treated with 70 µL

689   of transfection mix and incubated at 23°C for 24 hours. On the third day, the transfection medium

690   was removed and replaced with standard growth medium, and cells were allowed to recover for

691   24 hours. On the fourth day, growth medium was removed and replaced with medium

692   supplemented with selective drug (Geneticin at 320 µg/mL). Transfected cells were grown in

693   selective medium for two weeks changing media with fresh selective media every 3 days. Cells

25

694 in the negative control wells were dead after one week of drug selection. Red fluorescence from

695 tdTomato-positive cells was screened on an Olympus spinning disk confocal microscope using a

696 561 nm laser, which confirmed >99% of cells expressed tdTomato. After two weeks, the culture

697 of cells was expanded from a 24-well plate to 25 cm^2 culture flasks and maintained in selective

698 growth media until further use.

699

700 **Injection of fluorescent *Capsaspora* into snail tissue (related to Fig. 1C–D and Fig. S1C–D)**

701 Snails were prepared and mounted on microscope slides according to the BRI protocol.[69] Briefly,

702 snails measuring between 10 and 20 mm were placed in warm artificial pond water (70°C) for 50

703 seconds, then immediately submerged into a cold water bath for 60 seconds. Snails were

704 removed from their shell by gently pulling on the foot with forceps and placed on microscope

705 slides for injection. Snails were injected using glass capillary needles (World Precision

706 Instruments, 1B100F-6) pulled to an opening size of approximately 100 μm with a Model P-87

707 Sutter Instrument Micropipette Puller. Two days before the experiment, a 100% confluent flask of

708 *Capsaspora* cells stably expressing tdTomato were "fed" by replacing the selective growth media

709 with fresh selective growth media. The day before the experiment, the *Capsaspora* cells were

710 washed and resuspended in FBS-free media containing no antibiotics and allowed to starve

711 overnight. On the day of the experiment, cells were washed and then resuspended with Chernin's

712 balanced salt solution (CBSS+)[67] before injection. Snails were injected with 20 μL of *Capsaspora*

713 cells suspended in balanced salt solution ($4*10^7$ cells/mL) into their mantle cavity or pericardium.

714 After injection, needles were left in the tissue for several minutes to allow the hemolymph to clot

715 and prevent *Capsaspora* from bleeding back out. To determine if aggregation was calcium

716 dependent, the calcium chelator EGTA was pre-mixed with cells to a final concentration of 250

717 mM before injecting 20 μL into snails. As a negative control, cells were injected through the needle

718 directly onto a microscope slide with no snail. Also, snails that were never injected were imaged

719 (no red fluorescent cells of the correct size were observed). Red fluorescence was imaged using

720 an Olympus spinning disk confocal microscope with a 547 nm excitation laser. Brightfield and

721 green fluorescence (488 nm) images were taken as well to see surrounding snail tissue structure.

722

723 ***Capsaspora* forms multicellular aggregates in response to**
724 **macromolecules in host snail serum**

In vitro analysis of snail serum aggregation (related to Fig. 1E)

The standard aggregation assay on ultra-low attachment plates was used to assess activity of 100% (v/v) snail serum compared to 5% (v/v) FBS or 5% (v/v) 1X PBS. To test snail serum, FBS-free assay media was removed by aspiration and replaced with 100% 1X snail serum harvested by the headfoot retraction method. As controls, FBS-free assay media was removed and replaced with either media containing 5% (v/v) FBS or 5% (v/v) 1X PBS. Images of triplicate assay wells were taken every 30 minutes and example images are shown from T-90 minutes.

Snail serum fractionation (related to Fig. 1F–G)

Snail serum was fractionated using Amicon Ultra 30 kDa cutoff filters (Sigma, # UFC5030) according to the manufacturer's directions. Briefly, the filter was first washed with 500 μL of 1X PBS by centrifugation at 14,000xg for 15 minutes. Then 500 μL of harvested serum was added to the cutoff filter and centrifuged at 14,000xg for 15 minutes. The <30 kDa fraction was collected while the >30 kDa fraction was washed three more times with 1X PBS. The standard aggregation assay on ultra-low attachment plates was used to assess activity of 50% (v/v) whole unfractionated snail serum, 50% (v/v) >30 kDa snail serum, and 50% (v/v) <30 kDa snail serum, compared to 5% (v/v) FBS or 5% (v/v) 1X PBS. A dilution series of >30 kDa snail serum was also tested using this method. Images of triplicate assay wells were taken every 30 minutes and analysis was performed on images from T-90 minutes. Average aggregate areas were measured by batch processing with the FIJI macro script reported above.

Multiple strains of *Capsaspora* aggregate (related to Fig. 1H)

A non-standard aggregation assay using orbital agitation was set up. *Capsaspora* cells (ATCC $4*10^6$ cells/mL, M-line $8*10^6$ cells/mL, Salvador $8*10^6$ cells/mL) were washed and resuspended in growth media *without FBS,* hereafter referred to as *assay media,* and seeded into a 24-well plate (ATCC $2*10^6$ cells per well, M-line $4*10^6$ cells per well, Salvador $4*10^6$ cells per well). Aggregation inducers were added: 10% (v/v) FBS, 50% (v/v) >30 kDa snail serum, or 10% (v/v) PBS as a negative control), and the plate was agitated at 50 rpm overnight (Celltron Bench-Top Shaker, INFORS-HT). Aggregates were assessed by microscopy after ~11.5h. Average aggregate area was measured with the FIJI macro script described above.

756 **Morphological analysis of tdTomato expressing *Capsaspora* cells after 4 hours of**
757 **induction (related to Fig. 1I–O, Fig. 4A–P, and Fig. S2A/B/E)**

758 The standard aggregation assay was run using tdTomato expressing *Capsaspora* cells.
759 Aggregates were induced with either 5% (v/v) FBS or 50% (v/v) >30 kDa snail serum, or a dilution
760 series of pure DOPC vesicles (preparation described below) and 3D z-stacks were taken of each
761 replicate well monitored every 4 hours for 48 hours using a Cytation C10 imager (Agilent) with
762 confocal 546 nm excitation laser, laser autofocus, and a 20x objective. Three-dimensional z-
763 stacks from the time point after 4 hours of induction were analyzed using the Imaris batch
764 processing macro described below.

765

766 **Morphological Analysis of Propidium Iodide-stained Aggregates 14 hours after induction**
767 **(related to Fig. 1I–O, Fig. 4A–P, and Fig. S2C/D/F)**

768 *Capsaspora* aggregates were prepared following the standard aggregation assay protocol in ultra-
769 low attachment plates. Aggregates were induced with either 5% (v/v) FBS or 50% (v/v) >30 kDa
770 snail serum, or a dilution series of pure DOPC vesicles (preparation described below). About 14
771 hours after induction of aggregates, cells in assay plates were fixed with 4% (v/v) formaldehyde
772 for 30 minutes. Fixed aggregates were washed three times with 1X PBS and then stained with
773 0.02 mg/mL propidium iodide (PI) for 1 hour. Stained aggregates were washed three times with
774 1X PBS to remove excess PI before imaging. Cells were imaged using an Olympus spinning disk
775 confocal microscope with 546 nm excitation laser. Three-dimensional z-stacks of aggregates
776 were analyzed using the Imaris batch processing macro described below.

777

778 **Image analysis of 3D confocal experiments (related to Fig. 1I–O, Fig. 4B–P, and Fig. S2)**

779 Three-dimensional z-stacks of aggregates were analyzed by batch processing with Bitplane
780 Imaris Imaging Software version 10.0.1. Briefly, the batch protocol was as follows: create
781 Surfaces, surface grain size = 3 µm, manual threshold 82.114, add Spots, estimate diameter 3.51
782 µm, background subtraction, "Quality" above automatic threshold, classify spots based on
783 distance to surfaces, threshold 2.91 µm (inside surface), export statistics: surface sphericity,
784 surface intensity inside, number and classification of spots, surface area, surface volume, surface
785 bounding box oriented dimensions. A copy of the Imaris batch protocol is available upon request.

786

Aggregation dynamics over time (related to Fig. 2A–C, Fig. 4Q, and Movie S1–2)

The standard aggregation assay on ultra-low attachment plates was used to assess activity of 5% (v/v) FBS, 50% (v/v) >30 kDa snail serum, or 63 μg/mL DOPC vesicles over time. The corresponding volume of 1X PBS was used as a negative control. Plates were imaged every 20 minutes using the 4X objective on an Incucyte S3 Live-Cell Analysis System. Aggregates were induced 1 hour after initiating Incucyte reads, and plates were kept at 23°C by the system while incubating between images. Resulting image stacks from triplicate wells were first converted into binary and average aggregate area, as well as average aggregate circularity (calculated as the ratio of x and y bounding box dimensions), was calculated by batch processing with a macro script in FIJI adapted to analyze time stacks. Briefly, the macro is set to: set scale, make binary, gaussian blur (sigma = 4), run "analyze particles" size 3–100000, count, and summarize results. The summary results that were plotted were: average particle area, and circularity (calculated by the ratio of 2D bounding box dimensions). A copy of the FIJI stacks macro is available upon request. Representative binary images from selected time-points are shown.

801

Lipids extracted from snail serum are sufficient to trigger aggregation

Extraction of lipids from snail serum using butanol and diisopropyl ether (DIPE) (related to Fig. 3A–D)

Snail serum was harvested by the headfoot retraction method.[65] Lipids were extracted from serum following a protocol from Cham and Knowles (1976).[70] Briefly, 0.1 mg of EDTA was added to 1 mL of serum in a 4-dram vial. Then, 2.5 mL of premixed 25:75 (v/v) butanol to DIPE was added. The solution was rocked gently at a speed of 50 on a Fisherbrand Digital Platform Rocker for 3 hours. After rocking, the vials were allowed to sit for 15 minutes until the layers separated. The organic layer was carefully removed from the aqueous layer. Note that no proteins in the aqueous layer precipitated. The organic layer was completely evaporated using a Savant SpeedVac SPD2030 at 45°C under 5.1 millitorr of vacuum pressure for 2 hours. Lipids were extracted separately from the sera of three batches of snails and stored at –20°C until use.

814

Preparing lipid vesicles from lipid extracts or from pure lipid samples (related to Fig. 3 and Fig. 4)

Lipids extracted from snail serum samples or commercially obtained (pure synthetic lipids) were redissolved in chloroform in glass vials and transferred to a 1.7 mL microcentrifuge tube. The chloroform was evaporated using a gentle stream of nitrogen and the resulting lipid film was then resuspended in 1 mL each of 1X PBS. The tubes were vortexed for 30 seconds before sonication. Lipid solutions were sonicated on ice with a 50% duty cycle at medium setting for 10 minutes using a single probe attached to a Branson Sonifier Cell-Disruptor 185. During sonication, tubes were kept on ice and tube bottoms were set about 3 mm from the sonicator tip. Lipid solutions went from slightly cloudy to clear after sonication. Sonicated lipids were stored at 4°C for no more than 2 days before use. In the case of crude snail serum lipids (**Fig. 3A-D**), all the lipids were extracted from 1 mL of snail serum, resulting in ~ 0.3 mg of dried crude lipids. After extracting and drying, crude lipids were reconstituted in 1 mL of PBS buffer and sonicated. Therefore, the extracted lipids were present at their natural serum concentration. The resuspended lipids exhibited similar potency (v/v) as serum.

Testing lipid vesicles for aggregation (related to Fig. 3A,E,I,J)

Sonicated lipids were concentrated 10X using an Amicon Ultra 30 kDa cutoff filter and diluted with 1X PBS to the desired concentration before testing. The standard aggregation assay on ultra-low attachment plates was used to test for aggregation induction. Aggregates were induced using the desired lipid concentration (calculated in µg/mL of lipid) and 5% (v/v) of 1X PBS was used as a negative control. Aggregates in triplicate wells were imaged every 30 minutes and analysis was performed on images from T-90 minutes. Average aggregate areas were measured using a macro in FIJI as described above.

Transmission Electron Microscope (TEM) imaging of prepared lipid vesicles (related to Fig. 3B,F,K)

Before preparation of samples, Formvar/Carbon film 300 mesh Nickel Grids (Electron Microscopy Sciences FCF300-Ni-25) were ionized using a Pelco easiGlow Discharge System at 0.3 mbar and 15 mAmps for 2 minutes. 10 µL of prepared lipid samples were added to the ionized grids and allowed to sit for 5 minutes. Excess sample was removed from the grids by gently touching

846   Whatman filter paper (Sigma, WHA1001329) to the edge. Immediately after removing samples

847   (before grid dries) 10 µL of 2% (v/v) Uranyl Acetate pre-diluted in water was added to grids and

848   allowed to sit for 10 seconds. Then the stain was removed with the edge of Whatman filter paper.

849   Grids were allowed to dry completely before imaging (about 10 minutes). Prepared grids were

850   imaged using a JEOL-JEM 1010 transmission electron microscope (TEM) with an 80 kV operating

851   voltage, equipped with a 1k x 1k Gatan CCD camera (MegaScan model 794) using a tungsten

852   filament as its electron source.

853

854   **Determination of prepared lipid vesicle size using Dynamic Light Scattering (DLS) (related**

855   **to Fig. 3 C,G,L)**

856   400 µL of prepared lipid vesicles suspended in 1X PBS at room temperature were transferred to

857   a BRAND UV micro disposable cuvette (BR759200-100EA) and placed in a Malvern Panalytical

858   Zetasizer Nano ZS DLS. Size measurements were recorded in a range of 0.3 nm to 3 mm as raw

859   intensity and then normalized based on particle size using the Malvern software to give the final

860   distribution of particle sizes in each sample. The "number" distribution was plotted and Z-averages

861   (nm) were reported. Triplicate measurements were recorded for each sample.

862

863   **Mass spectrometric analysis of lipid samples (related to Fig. 3D,H, Fig. 5D–F, Fig. 6C–E,**

864   **Fig. S3, and Table S1)**

865   For most lipidomics analysis, fully dried lipid samples were shipped to the Beth Israel Deaconess

866   Medical Center (BIDMC) Metabolomics Core. The LC-MS/MS based non-polar lipidomics profiling

867   work was conducted by Dr. John Asara at the BIDMC Mass Spectrometry Core in Boston, MA

868   USA. For calculation of the amount of DOPC in snail serum samples, 1 mL of snail serum was

869   spiked with a known volume of SPLASH Lipidomix II mass spectrometry standard (Avanti Polar

870   Lipids, #330709) and then extracted according to the method described above. Dried lipid

871   samples were resuspended in 2:1 (v/v) isopropanol/methanol. High-resolution electrospray

872   ionization (HR-ESI) mass spectra with collision-induced dissociation (CID) MS/MS were obtained

873   using an Agilent LC-q-TOF mass spectrometer 6530 equipped with an Agilent 1290 uHPLC

874   system. Metabolites were separated using a Luna 5 µm C5 100 Å LC column (Phenomenex 00D-

875   4043-E0). Mobile phase A was 95% (v/v) Water, 5% (v/v) Methanol, 0.1% (v/v) Formic Acid, and

876   5 mM Ammonium Formate. Mobile phase B was 60% (v/v) Isopropanol, 35% (v/v) Methanol, 5%

31

877   (v/v) Water, 0.1% (v/v) Formic Acid, and 5 mM Ammonium Formate. After initially holding 0%

878   phase B for 5 min at 0.1 mL/min, a linear gradient from 20% phase B to 100% phase B was

879   applied over 40 min with a flow of 0.4 mL/min before holding at 100% phase B for another 5 min

880   with a flow of 0.5 mL/min. Data-dependent acquisition was employed to fragment the top masses

881   in each scan. Collision-induced dissociation was applied using a linear formula that applied a

882   higher voltage for larger molecules (CID voltage = 10 + 0.02 m/z)for metabolite profiling and

883   identification. Mass traces collected in positive mode were analyzed in MassLynx software v4.1

884   and calculated concentrations were normalized to the known concentration of the internal

885   SPLASH standard.

886

Capsaspora responds to host infection with *Schistosoma mansoni*

Infection of M-line snails with PR1 schistosomes (related to Fig. 5 and Fig. 6)

889   Two mice were exposed to 150 PR1 (Puerto Rican Strain 1) cercariae from snails originally

890   exposed to BRI-derived miracidia, the resulting miracidia from those two mice were used to

891   expose 120 5-6 mm *B. glabrata* M-line snails to 10 PR1 miracidia. All miracidia displayed positive

892   phototaxis, normal shape, and swimming behavior. Snails were exposed for 2 hours in 12-well

893   cell culture plates and then placed into 4 different 20 L tanks. 60 5-6 mm *B. glabrata* M-line snails

894   were sham-exposed (no parasites) in 12-well cell culture plates for 2 hours and placed into 3

895   different 20 L tanks as control snails. Experimental snails were fed 3 times a week red leaf lettuce

896   and 2 Wardly® shrimp pellets. Snails were maintained between 25-27ºC on a 12h:12h light-dark

897   cycle. After 28, 32 and 38 days post-exposure, snails were checked to determine if cercariae were

898   being released (shedding). Snails were placed in 12-well cell culture plates for 2 hours between

899   10:00 am to 12:00 pm under light. At 38 days post-exposure, 79 *B. glabrata* M-line snails were

900   shedding cercariae (group 1: n=20, group 2: n=20, group 3: n=20, group 4: n=19). Sham-exposed

901   control snails were in 3 different groups (group 1: n=20, group 2: n=20, group 3: n=11).

902

Measuring aggregation induced by naïve and infected M-line snail serum and naïve NMRI snail serum (related to Fig. 5A–C and Fig. 6A–B)

905   The standard aggregation assay using ultra-low attachment plates was used to determine

906   aggregation potency of snail serum samples. Serum collected from three separate batches of

907   naïve or infected snails were each concentrated to 5X using an Amicon Ultra 30 kDa cutoff filter.

908   Aggregation was induced by a dilution series of each of the >30 kDa snail serum samples. Assay

909   wells were imaged every 30 minutes and representative images from T90 minutes are shown.

910   Average aggregate area was calculated by batch processing with the standard macro script in

911   FIJI as described above.

912

913

914   ## *Capsaspora* responds differently to serum of different *Biomphalaria*

915   ## strains

916   **Proteomics analysis of snail serum samples (related to Fig. 6E, Fig. S4, and Table S2)**

917   Serum harvested from three separate batches of naïve NMRI, naïve M-line, and infected M-line

918   snails via the headfoot retraction method were submitted for untargeted proteomics analysis by

919   the Laboratory for Biological Mass Spectrometry at Indiana University.

References

1 McFall-Ngai, M. *et al.* Animals in a bacterial world, a new imperative for the life sciences. *Proceedings of the National Academy of Sciences* **110**, 3229-3236 (2013). https://doi.org:doi:10.1073/pnas.1218525110

2 Drew, G. C., Stevens, E. J. & King, K. C. Microbial evolution and transitions along the parasite–mutualist continuum. *Nature Reviews Microbiology* **19**, 623-638 (2021). https://doi.org:10.1038/s41579-021-00550-7

3 del Campo, J., Bass, D. & Keeling, P. J. The eukaryome: Diversity and role of microeukaryotic organisms associated with animal hosts. *Functional Ecology* **34**, 2045-2054 (2020). https://doi.org:https://doi.org/10.1111/1365-2435.13490

4 Fisher, M. C. *et al.* Emerging fungal threats to animal, plant and ecosystem health. *Nature* **484**, 186-194 (2012). https://doi.org:10.1038/nature10947

5 Du, H. *et al.* Candida auris: Epidemiology, biology, antifungal resistance, and virulence. *PLoS Pathog* **16**, e1008921 (2020). https://doi.org:10.1371/journal.ppat.1008921

6 Akhoundi, M. *et al.* A Historical Overview of the Classification, Evolution, and Dispersion of Leishmania Parasites and Sandflies. *PLOS Neglected Tropical Diseases* **10**, e0004349 (2016). https://doi.org:10.1371/journal.pntd.0004349

7 Cowman, A. F., Healer, J., Marapana, D. & Marsh, K. Malaria: Biology and Disease. *Cell* **167**, 610-624 (2016). https://doi.org:https://doi.org/10.1016/j.cell.2016.07.055

8 Lin, S. *et al.* The *Symbiodinium kawagutii* genome illuminates dinoflagellate gene expression and coral symbiosis. *Science* **350**, 691-694 (2015). https://doi.org:doi:10.1126/science.aad0408

9 Kittelmann, S. *et al.* Phylogeny of Intestinal Ciliates, Including Charonina ventriculi, and Comparison of Microscopy and 18S rRNA Gene Pyrosequencing for Rumen Ciliate Community Structure Analysis. *Applied and Environmental Microbiology* **81**, 2433-2444 (2015). https://doi.org:doi:10.1128/AEM.03697-14

10 Chudnovskiy, A. *et al.* Host-Protozoan Interactions Protect from Mucosal Infections through Activation of the Inflammasome. *Cell* **167**, 444-456.e414 (2016). https://doi.org:https://doi.org/10.1016/j.cell.2016.08.076

11 Hertel, L. A., Bayne, C. J. & Loker, E. S. The symbiont Capsaspora owczarzaki, nov. gen. nov. sp., isolated from three strains of the pulmonate snail Biomphalaria glabrata is related to members of the Mesomycetozoea. *International Journal for Parasitology* **32**, 1183-1191 (2002). https://doi.org:https://doi.org/10.1016/S0020-7519(02)00066-8

12 Stibbs, H. H., Owczarzak, A., Bayne, C. J. & DeWan, P. Schistosome sporocyst-killing Amoebae isolated from Biomphalaria glabrata. *J Invertebr Pathol* **33**, 159-170 (1979). https://doi.org:10.1016/0022-2011(79)90149-6

13 Harry, H. W. & Aldrich, D. V. The ecology of Australorbis glabratus in Puerto Rico. *Bull World Health Organ* **18**, 819-832 (1958).

14 Stirewalt, M. A. Effect of snail maintenance temperatures on development of Schistosoma mansoni. *Exp Parasitol* **3**, 504-516 (1954). https://doi.org:10.1016/0014-4894(54)90046-6

15 Pimentel, D. Life History of Australorbis Glabratus, The Intermediate Snail Host of Schistosoma Mansoni in Puerto Rico. *Ecology* **38**, 576-580 (1957). https://doi.org:https://doi.org/10.2307/1943122

16 Lewis, F. A., Stirewalt, M. A., Souza, C. P. & Gazzinelli, G. Large-scale laboratory maintenance of Schistosoma mansoni, with observations on three schistosome/snail host combinations. *J Parasitol* **72**, 813-829 (1986).

17   Adema, C. M. *et al.* Will All Scientists Working on Snails and the Diseases They Transmit Please Stand Up? *PLOS Neglected Tropical Diseases* **6**, e1835 (2012). https://doi.org:10.1371/journal.pntd.0001835

18   Sebé-Pedrós, A. *et al.* The Dynamic Regulatory Genome of Capsaspora and the Origin of Animal Multicellularity. *Cell* **165**, 1224-1237 (2016). https://doi.org:10.1016/j.cell.2016.03.034

19   Ferrer-Bonet, M. & Ruiz-Trillo, I. *Capsaspora owczarzaki*. *Current Biology* **27**, R829-R830 (2017). https://doi.org:10.1016/j.cub.2017.05.074

20   Pérez-Posada, A., Dudin, O., Ocaña-Pallarès, E., Ruiz-Trillo, I. & Ondracka, A. Cell cycle transcriptomics of Capsaspora provides insights into the evolution of cyclin-CDK machinery. *PLOS Genetics* **16**, e1008584 (2020). https://doi.org:10.1371/journal.pgen.1008584

21   Sebé-Pedrós, A. *et al.* High-Throughput Proteomics Reveals the Unicellular Roots of Animal Phosphosignaling and Cell Differentiation. *Developmental Cell* **39**, 186-197 (2016). https://doi.org:https://doi.org/10.1016/j.devcel.2016.09.019

22   Suga, H. *et al.* The Capsaspora genome reveals a complex unicellular prehistory of animals. *Nat Commun* **4**, 2325 (2013). https://doi.org:10.1038/ncomms3325

23   Sebé-Pedrós, A. *et al.* Regulated aggregative multicellularity in a close unicellular relative of metazoa. *eLife* **2**, e01287 (2013). https://doi.org:10.7554/eLife.01287

24   Parra-Acero, H. *et al.* Integrin-Mediated Adhesion in the Unicellular Holozoan Capsaspora owczarzaki. *Curr Biol* **30**, 4270-4275.e4274 (2020). https://doi.org:10.1016/j.cub.2020.08.015

25   Parra-Acero, H. *et al.* Transfection of Capsaspora owczarzaki, a close unicellular relative of animals. *Development* **145** (2018). https://doi.org:10.1242/dev.162107

26   Phillips, J. E., Santos, M., Konchwala, M., Xing, C. & Pan, D. Genome editing in the unicellular holozoan Capsaspora owczarzaki suggests a premetazoan role for the Hippo pathway in multicellular morphogenesis. *eLife* **11**, e77598 (2022). https://doi.org:10.7554/eLife.77598

27   Ros-Rocher, N. *et al.* Chemical factors induce aggregative multicellularity in a close unicellular relative of animals. *Proceedings of the National Academy of Sciences* **120**, e2216668120 (2023). https://doi.org:doi:10.1073/pnas.2216668120

28   Owczarzak, A., Stibbs, H. H. & Bayne, C. J. The destruction of Schistosoma mansoni mother sporocysts in vitro by amoebae isolated from Biomphalaria glabrata: an ultrastructural study. *J Invertebr Pathol* **35**, 26-33 (1980). https://doi.org:10.1016/0022-2011(80)90079-8

29   Utarini, A. *et al.* Efficacy of Wolbachia-Infected Mosquito Deployments for the Control of Dengue. *New England Journal of Medicine* **384**, 2177-2186 (2021). https://doi.org:10.1056/NEJMoa2030243

30   Moreira, L. A. *et al.* A *Wolbachia* Symbiont in *Aedes aegypti* Limits Infection with Dengue, Chikungunya, and *Plasmodium*. *Cell* **139**, 1268-1278 (2009). https://doi.org:10.1016/j.cell.2009.11.042

31   Bian, G. *et al.* *Wolbachia* Invades *Anopheles stephensi* Populations and Induces Refractoriness to *Plasmodium* Infection. *Science* **340**, 748-751 (2013). https://doi.org:doi:10.1126/science.1236192

32   Evan Secor, W. Water-based interventions for schistosomiasis control. *Pathog Glob Health* **108**, 246-254 (2014). https://doi.org:10.1179/2047773214y.0000000149

33   McCullough, F. S., Gayral, P., Duncan, J. & Christie, J. D. Molluscicides in schistosomiasis control. *Bull World Health Organ* **58**, 681-689 (1980).

34   Laidemitt, M. R. *et al.* Antagonism between parasites within snail hosts impacts the transmission of human schistosomiasis. *eLife* **8**, e50095 (2019). https://doi.org:10.7554/eLife.50095

35   Bayne, C. J. Lectin-induced mitogenesis of cytotoxic amebae (Nuclearia) isolated from Biomphalaria glabrata (Mollusca: Gastropoda). *Developmental & Comparative Immunology* **6**, 369-373 (1982). https://doi.org:https://doi.org/10.1016/S0145-305X(82)80020-7

1012   36   Buddenborg, S. K. *et al.* Transcriptomic responses of Biomphalaria pfeifferi to Schistosoma
1013   mansoni: Investigation of a neglected African snail that supports more S. mansoni transmission
1014   than any other snail species. *PLOS Neglected Tropical Diseases* **11**, e0005984 (2017).
1015   https://doi.org:10.1371/journal.pntd.0005984

1016   37   Phillips, J. E. & Pan, D. The Hippo kinase cascade regulates a contractile cell behavior and cell
1017   density in a close unicellular relative of animals. *bioRxiv*, 2023.2007.2025.550562 (2023).
1018   https://doi.org:10.1101/2023.07.25.550562

1019   38   Fried, B., Cahn-Hidalgo, D., Fujino, T. & Sherma, J. Diet-Induced Differences in the Distribution of
1020   Neutral Lipids in Selected Organs of Biomphalaria glabrata (Gastropoda: Planorbidae) as
1021   Determined by Thin-Layer Chromatography and Light and Electron Microscopy. *Transactions of
1022   the American Microscopical Society* **110**, 163-171 (1991). https://doi.org:10.2307/3226752

1023   39   Aloisi, J. D., Fried, B. & Sherma, J. Reversal of dietary-induced hyperlipidemia in Biomphalaria
1024   glabrata (Gastropoda). *Comp Biochem Physiol A Comp Physiol* **100**, 203-204 (1991).
1025   https://doi.org:10.1016/0300-9629(91)90208-t

1026   40   Tunholi-Alves, V. M. *et al.* Lipid levels in Biomphalaria glabrata infected with different doses of
1027   Echinostoma   paraensei   miracidia.   *Exp   Parasitol*   **128**,   212-216   (2011).
1028   https://doi.org:10.1016/j.exppara.2011.03.009

1029   41   Bandstra, S. R., Fried, B. & Sherma, J. High-performance thin-layer chromatographic analysis of
1030   neutral lipids and phospholipids in Biomphalaria glabrata patently infected with Echinostoma
1031   caproni. *Parasitology Research* **99**, 414-418 (2006). https://doi.org:10.1007/s00436-006-0180-5

1032   42   Ray, C. L. *et al.* Effect of dietary phytase on water and fecal prokaryotic and eukaryotic
1033   microbiomes in a hybrid tilapia (*Oreochromis aureus* x *O. niloticus*) mixotrophic biofloc production
1034   system. *Aquaculture* **581** (2024). https://doi.org:10.1016/j.aquaculture.2023.740433

1035   43   Hanington, P. C. & Zhang, S. M. The primary role of fibrinogen-related proteins in invertebrates is
1036   defense, not coagulation. *J Innate Immun* **3**, 17-27 (2011). https://doi.org:10.1159/000321882

1037   44   Adema, C. M. Fibrinogen-Related Proteins (FREPs) in Mollusks. *Results Probl Cell Differ* **57**, 111-
1038   129 (2015). https://doi.org:10.1007/978-3-319-20819-0_5

1039   45   Lu, L., Loker, E. S., Adema, C. M., Zhang, S. M. & Bu, L. Genomic and transcriptional analysis of
1040   genes containing fibrinogen and IgSF domains in the schistosome vector *Biomphalaria glabrata*,
1041   with emphasis on the differential responses of snails susceptible or resistant to *Schistosoma
1042   mansoni*. *PLoS Negl Trop Dis* **14**, e0008780 (2020). https://doi.org:10.1371/journal.pntd.0008780

1043   46   Faizullin, D., Valiullina, Y., Salnikov, V. & Zuev, Y. Direct interaction of fibrinogen with lipid
1044   microparticles modulates clotting kinetics and clot structure. *Nanomedicine: Nanotechnology,
1045   Biology   and   Medicine   **23**,   102098   (2020).
1046   https://doi.org:https://doi.org/10.1016/j.nano.2019.102098

1047   47   Bao, J. *et al.* Serpin functions in host-pathogen interactions. *PeerJ* **6**, e4557 (2018).
1048   https://doi.org:10.7717/peerj.4557

1049   48   Herron, M. D., Conlin, P. L. & Ratcliff, W. C. *The evolution of multicellularity*. First edition. edn,
1050   (CRC Press, 2022).

1051   49   Lyons, N. A. & Kolter, R. On the evolution of bacterial multicellularity. *Curr Opin Microbiol* **24**, 21-
1052   28 (2015). https://doi.org:10.1016/j.mib.2014.12.007

1053   50   Bonner, J. T. The origins of multicellularity. *Integrative Biology: Issues, News, and Reviews* **1**, 27-
1054   36   (1998).   https://doi.org:https://doi.org/10.1002/(SICI)1520-6602(1998)1:1<27::AID-
1055   INBI4>3.0.CO;2-6

1056   51   Darch, S. E., West, S. A., Winzer, K. & Diggle, S. P. Density-dependent fitness benefits in quorum-
1057   sensing bacterial populations. *Proceedings of the National Academy of Sciences* **109**, 8259-8263
1058   (2012). https://doi.org:10.1073/pnas.1118131109

1059 52 Justice, S. S., Hunstad, D. A., Cegelski, L. & Hultgren, S. J. Morphological plasticity as a bacterial survival strategy. *Nature Reviews Microbiology* **6**, 162-168 (2008). https://doi.org:10.1038/nrmicro1820

1062 53 Roilides, E., Simitsopoulou, M., Katragkou, A. & Walsh, T. J. How Biofilms Evade Host Defenses. *Microbiology Spectrum* **3**, 10.1128/microbiolspec.mb-0012-2014 (2015). https://doi.org:doi:10.1128/microbiolspec.mb-0012-2014

1065 54 Herron, M. D. *et al.* De novo origins of multicellularity in response to predation. *Sci Rep* **9**, 2328 (2019). https://doi.org:10.1038/s41598-019-39558-8

1067 55 Kapsetaki, S. E. & West, S. A. The costs and benefits of multicellular group formation in algae*. *Evolution* **73**, 1296-1308 (2019). https://doi.org:10.1111/evo.13712

1069 56 Loker, E. S., Bayne, C. J., Buckley, P. M. & Kruse, K. T. Ultrastructure of encapsulation of Schistosoma mansoni mother sporocysts by hemocytes of juveniles of the 10-R2 strain of Biomphalaria glabrata. *J Parasitol* **68**, 84-94 (1982).

1072 57 Castillo, M. G. *et al.* Biomphalaria glabrata immunity: Post-genome advances. *Developmental & Comparative Immunology* **104**, 103557 (2020). https://doi.org:https://doi.org/10.1016/j.dci.2019.103557

1075 58 Galinier, R. *et al.* Biomphalysin, a new β pore-forming toxin involved in Biomphalaria glabrata immune defense against Schistosoma mansoni. *PLoS Pathog* **9**, e1003216 (2013). https://doi.org:10.1371/journal.ppat.1003216

1078 59 Ferrer-Bonet, M. & Ruiz-Trillo, I. *Capsaspora owczarzaki*. *Current Biology* **27**, R829-R830 (2017). https://doi.org:10.1016/j.cub.2017.05.074 PMID - 28898640

1080 60 Ruiz-Trillo, I., Kin, K. & Casacuberta, E. The origin of metazoan multicellularity: a potential microbial black swan event. *Annu. Rev. Microbiol.* **77**, 499-516 (2023). https://doi.org:10.1146/annurev-micro-032421-120023

1083 61 Hehenberger, E. *et al.* Novel Predators Reshape Holozoan Phylogeny and Reveal the Presence of a Two-Component Signaling System in the Ancestor of Animals. *Current Biology* **27**, 2043-2050.e2046 (2017). https://doi.org:https://doi.org/10.1016/j.cub.2017.06.006

1086 62 Tong, S. M. Heterotrophic flagellates and other protists from Southampton Water, U.K. *Ophelia* **47**, 71-131 (1997). https://doi.org:10.1080/00785236.1997.10427291

1088 63 Urrutia, A. *et al. Txikispora philomaios* n. sp., n. g., a micro-eukaryotic pathogen of amphipods, reveals parasitism and hidden diversity in Class Filasterea. *J Eukaryot Microbiol* **69**, e12875 (2022). https://doi.org:10.1111/jeu.12875

1091 64 Tikhonenkov, D. V. *et al.* New Lineage of Microbial Predators Adds Complexity to Reconstructing the Evolutionary Origin of Animals. *Current Biology* **30**, 4500-4509.e4505 (2020). https://doi.org:https://doi.org/10.1016/j.cub.2020.08.061

1094 65 Sminia, T. & Barendsen, L. A comparative morphological and enzyme histochemical study on blood cells of the freshwater snails Lymnaea stagnalis, Biomphalaria glabrata, and Bulinus truncatus. *Journal of Morphology* **165**, 31-39 (1980). https://doi.org:https://doi.org/10.1002/jmor.1051650104

1098 66 Gilbertson, C. R. & Wyatt, J. D. Evaluation of Euthanasia Techniques for an Invertebrate Species, Land Snails (Succinea putris). *J Am Assoc Lab Anim Sci* **55**, 577-581 (2016).

1100 67 Chernin, E. Observations on hearts explanted in vitro from the snail Australorbis glabratus. *J Parasitol* **49**, 353-364 (1963).

1102 68 Schindelin, J. *et al.* Fiji: an open-source platform for biological-image analysis. *Nature Methods* **9**, 676-682 (2012). https://doi.org:10.1038/nmeth.2019

1104 69 Sereno, F. L. a. M. *Fixing Biomphalaria glabrata snails for dissection*, <https://www.afbr-bri.org/schistosomiasis/standard-operating-procedures/fixing-biomphalaria-glabrata-snails-for-dissection/> (2023).

1107   70   Cham, B. E. & Knowles, B. R. A solvent system for delipidation of plasma or serum without protein
1108   precipitation.   *Journal   of   Lipid   Research*   **17**,   176-181   (1976).
1109   https://doi.org:https://doi.org/10.1016/S0022-2275(20)37003-6

1110